

DOT/FAA/AR-09/14

Office of Airport Safety & Standards
(Air Traffic Organization
Operations Planning)
Office of Aviation Research
and Development
Washington, DC 20591

EMAS Cold Weather Performance Investigations

September 2009

Final Report

The research described in this report was funded by the FAA as part of its mission to improve aircraft safety. The views and opinions expressed are those of the author alone and do not necessarily represent the views of the FAA. The FAA assumes no liability for the contents or use thereof. The FAA has not edited or modified the contents of the report in any manner.

This document is available to the U.S. public through the National Technical Information Services (NTIS), Springfield, Virginia 22161.



U.S. Department of Transportation
Federal Aviation Administration

NOTICE

This document is disseminated under the sponsorship of the U.S. Department of Transportation in the interest of information exchange. The United States Government assumes no liability for the contents or use thereof. The United States Government does not endorse products or manufacturers. Trade or manufacturer's names appear herein solely because they are considered essential to the objective of this report. This document does not constitute FAA certification policy. Consult your local FAA airports office as to its use.

This report is available at the Federal Aviation Administration William J. Hughes Technical Center's Full-Text Technical Reports page: actlibrary.act.faa.gov in Adobe Acrobat portable document format (PDF).

Technical Report Documentation Page

1. Report No. DOT/FAA/AR-09/14		2. Government Accession No.		3. Recipient's Catalog No.	
4. Title and Subtitle EMAS COLD WEATHER PERFORMANCE INVESTIGATIONS				5. Report Date September 2009	
				6. Performing Organization Code	
7. Author(s) Barry A. Coutermarsh				8. Performing Organization Report No. ERDC/CRREL Letter Report 08-09	
9. Performing Organization Name and Address U.S. Army Corps of Engineers Engineer Research and Development Center Cold Regions Research and Engineering Laboratory (CRREL) 72 Lyme Road Hanover, NH 03755-1290				10. Work Unit No. (TRAVIS)	
				11. Contract or Grant No.	
12. Sponsoring Agency Name and Address U.S. Department of Transportation Federal Aviation Administration Office of Airport Safety & Standards (Air Traffic Organization Operations Planning) Office of Aviation Research and Development Washington, DC 20591				13. Type of Report and Period Covered Final Report	
				14. Sponsoring Agency Code AAS-100	
15. Supplementary Notes <p>This effort was performed through an Interagency Agreement between the FAA and the U.S. Army Corps of Engineers Cold Regions Research and Engineering Laboratory in cooperation with Engineering System's Corporation through a Cooperative Research and Development Agreement. This report is the same report published by CRREL on October 2008 under the title EMAS Cold Weather Performance Investigations.</p>					
16. Abstract <p>At some airports, Engineered Material Arresting Systems (EMAS) are used in runway safety areas at to provide a mechanism for decelerating aircraft in the event of a runway overrun. The main component of an EMAS is energy-absorbing cellular concrete material that is relatively delicate. A system of sealants, coatings, and outer layers protect the cellular concrete from environmental conditions such as weather and jet blast. A research study was conducted to ascertain an EMAS's durability in cold climates where temperatures cycle between freezing and thawing. Four series of tests were performed, including (1) thermal cycling on a large-scale EMAS bed, (2) temperature and humidity cycling on 1-cubic-foot EMAS samples, (3) adhesion tests on EMAS sealant materials, and (4) durability tests on the materials that comprise the top protective layer of EMAS blocks.</p> <p>The large-scale EMAS bed was thermally cycled from -20°F to room temperature for 20 cycles over a 9-month period. Qualitative condition assessments were performed during the cycling, and quantitative post-cycling punch tests were performed and compared to the pre-cycling punch tests.</p> <p>Overall, the large-scale test showed the EMAS system tolerated the cold cycling well with little change in punch strength. The moisture present in the seams appeared not to have deteriorated the EMAS over the length of this cycling, but there was a significant amount of frost found during the cold inspections at the bed teardown.</p> <p>The EMAS samples tolerated the cold and humidity tests with no significant punch strength change. Generally, both seam tapes performed well in the cold, with a tensile strength increase. The block tops also showed a slight puncture strength increase with decreasing temperature.</p>					
17. Key Words EMAS, Cellular concrete, Freeze-thaw cycle, Durability, Punch test			18. Distribution Statement This document is available to the U.S. public through the National Technical Information Service (NTIS), Springfield, Virginia 22161.		
19. Security Classif. (of this report) Unclassified		20. Security Classif. (of this page) Unclassified		21. No. of Pages 63	22. Price



EMAS Cold Weather Performance Investigations

Barry A. Coutermarsh

October 2008

EMAS Cold Weather Performance Investigations

Barry A. Coutermarsh

*US Army Engineer Research and Development Center
Cold Regions Research and Engineering Laboratory
72 Lyme Road
Hanover, New Hampshire 03755-1290*

Approved for public release; distribution is unlimited.

Contents

Figures and Tables.....	iv
1 Introduction.....	1
2 Testing Facilities.....	2
3 Executive Summary	3
Large-scale bed cycling.....	3
Temperature and humidity cycling.....	3
Seam tape adhesion tests.....	3
Top durability tests	4
Overall.....	4
4 EMAS Description	6
5 Study Rationale and Test Descriptions	10
Large-scale bed cycling.....	11
<i>Instrumentation</i>	11
<i>Temperature discussion</i>	15
<i>Humidity discussion</i>	19
<i>Cold inspections</i>	24
<i>Qualitative block inspections.....</i>	29
<i>Qualitative system inspections</i>	31
<i>Vents.....</i>	31
<i>Seam tape</i>	31
<i>Sealant at vents.....</i>	32
Quantitative block punch data	35
<i>Punch procedure</i>	35
<i>Punch test discussion</i>	36
Temperature and humidity cycling tests	40
<i>Humidity test discussion</i>	42
Seam tape adhesion tests.....	42
<i>Seam tape test discussion</i>	44
Top durability tests	49
<i>"Tool-drop" test discussion.....</i>	50

Figures and Tables

Figures

Figure 1. EMAS bed at Chicago Midway Airport.....	6
Figure 2. EMAS 4-ft × 4-ft × 20-inch-thick block.....	7
Figure 3. Side view of EMAS bed being installed for testing at CRREL.....	7
Figure 4. Butyl and tedlar tape being applied to gap between blocks.....	8
Figure 5. Silicone seam tape applied to gaps between EMAS boards.....	8
Figure 6. Side flashing applied to exposed side of EMAS.....	9
Figure 7. Plastic vent in vertical part of gap between EMAS blocks.....	9
Figure 8. Overall EMAS bed layout with row and column numbers and sensor locations.....	12
Figure 9. Detail view of the EMAS bed sensor layout with sensor labels.....	13
Figure 10. Precon temperature/RH sensor and a thermocouple (red tip) mounted on the side of a block.....	13
Figure 11. Thermocouple layout used in the instrumented center and edge blocks.....	13
Figure 12. Campbell datalogging system.....	14
Figure 13. Ambient, in-block, and beneath-block temperatures for Julian days 300–330.....	16
Figure 14. Seam temperatures from thermocouples F1–F4, Julian days 300–330.....	16
Figure 15. Seam temperatures from thermocouples F5–F8 for Julian days 300–330.....	17
Figure 16. Temperatures measured by the Precon sensors at four vent locations and an interior seam, Julian days 300–330.....	17
Figure 17. EMAS block being installed showing locations of thermocouple (at left) and Precon temperature/relative humidity sensor nearer where the vent eventually will be installed.....	19
Figure 18. Ambient temperature and RH over EMAS bed during cycling.....	20
Figure 19. Smoothed relative humidity at the start of cycling.....	21
Figure 20. Temperatures measured by the temp/RH sensors Vent 1–Vent 4, RH1 and under a block at the beginning of cycling.....	22
Figure 21. Smoothed relative humidity data, Julian days 300–330.....	23
Figure 22. Five seam temperatures with ambient for Julian days 300–330.....	23
Figure 23. Small amount of frost along underside of sealing tape, row 5, column 20.....	25
Figure 24. Frost where the 8-inch and 14-inch blocks meet.....	25
Figure 25. Slightly more frost between 14-inch-thick blocks in column 19 than found in column 20.....	26
Figure 26. Frost between 14-inch- and 20-inch-thick blocks.....	26
Figure 27. Typical frost pattern on the side of a block.....	27
Figure 28. Frost distribution shows an increase at the corners.....	27
Figure 29. Decreasing frost at some corners.....	28

Figure 30. Thicker frost at the intersection of four blocks	28
Figure 31. Frost in a vent from the first level of 8-inch-thick blocks	29
Figure 32. Frost in the second-level vents.	29
Figure 33. Underside of block top with frost traces	30
Figure 34. Sample removed from material directly under the block top	30
Figure 35. Sample cutout from a block side that had surface frost on it.....	31
Figure 36. Vent frosting completely plugging the vent	32
Figure 37. Front view of vent shown in Figure 36 with frost plugging holes.....	32
Figure 38. Tedlar/butyl tape showing some splitting and shrinkage	33
Figure 39. Flashing tearing above vent.....	34
Figure 40. Vent sealant pulling away from flashing.....	34
Figure 41. Sealant at vent pulling from flashing.....	35
Figure 42. CRREL Punch Tester with an EMAS block in place.....	36
Figure 43. Top view of EMAS block showing punch test locations.....	36
Figure 44. Typical stress versus displacement fraction curve from the block punch data.....	38
Figure 45. Average stress at 35% displacement fraction pre- and post-thermal cycling comparison	39
Figure 46. Average maximum stress pre- and post-thermal cycling comparison	39
Figure 47. Average maximum linear stress pre- and post-thermal cycling comparison	40
Figure 48. Average linear fit slope pre- and post-thermal cycling comparison	40
Figure 49. CRREL temperature chamber.....	41
Figure 50. Temperature and humidity example	42
Figure 51. Punch test results for the temperature and humidity testing	43
Figure 52. Sealing tape coupon mounted in test fixture.....	44
Figure 53. Tedlar/butyl force displacement plot for room temp and - 50° F	45
Figure 54. Summary of all Tedlar/butyl tape tests	45
Figure 55. Tedlar/butyl tested at room temperature shows the Tedlar sliding from the butyl mastic	46
Figure 56. Tedlar/butyl tape tested at a cold temperature showing failure within the Tedlar film and no evidence of sliding off the mastic.....	46
Figure 57. Silicone sealing tape force/displacement graph for room and -50° F temperatures.....	47
Figure 58. Silicone seam tape summary for all temperatures.....	48
Figure 59. Silicone seam tape at failure. There is no tape slippage from the top material	48
Figure 60. Eyebolt drop indenter	49
Figure 61. Spherical drop indenter	50
Figure 62. Damage volume versus drop energy for the eyebolt indenter	52
Figure 63. Damage volume versus drop energy for the spherical indenter	52

Tables

Table 1. Temperature ranges and means throughout the block thickness from the center and edge blocks, Julian days 300–330	18
Table 2. Range and mean seam temperatures for all cycles	18
Table 3. Relative humidity from all the RH sensors for all cycles.....	24
Table 4. Pre- and post-cycling stress and slope values	38
Table 5. Test conditions for the sealing tape adhesion tests.....	44
Table 6. Tool drop indenter specifications	50
Table 7. Average tool drop kinetic energy and damage volume results	51

EMAS Cold Weather Performance Investigations

Barry A. Coutermarsh

1 Introduction

Ryan King, Project Manager, Federal Aviation Administration (FAA) Airport Safety R&D Section; and Daniel Edwards, Vice President, Installation, Maintenance, Repair and Overhaul Services, Engineered Arresting Systems Corporation (ESCO), a manufacturer of Engineered Material Arresting Systems (EMAS), approached the Cold Regions Research and Engineering Laboratory (CRREL) in 2007 to discuss performing cold weather durability studies on their Engineered Material Arresting System (EMAS).

FAA and ESCO guidance regarding the type of testing desired was as follows:

- A large-scale EMAS test to reflect cold environmental conditions was a primary priority.
- Tests were to reflect service conditions normally found where the bed would be installed.
- Classic material tests *per se* were not desired.

2 Testing Facilities

Established in 1961 with the merger of two Corps of Engineers research laboratories focused on snow, ice, and permafrost, and impacts on Arctic construction, CRREL has pioneered cold regions research and engineering solutions for more than 45 years, solving critical problems for the Army, the Department of Defense, and the Nation. Today, CRREL offers unique scientific research capabilities and resources. These include specialized physical facilities, equipment, instrumentation, scientific expertise, and operations personnel available for use by its research customers and partners. CRREL's technical staff is internationally recognized for its expertise; 40% of the staff have PhDs and 45% have masters degrees. CRREL staff members regularly publish in specialized journals, e.g., *Journal of the Acoustical Society of America*, *Journal of Terramechanics*, *Journal of Geophysical Research*, and *Cold Regions Science and Technology*. The Technology Information Analysis Center is the Nation's corporate repository for data generated within the cold regions area of science and engineering.

The principal experimental and laboratory facilities operated by CRREL are located at the headquarters complex at Hanover, New Hampshire. CRREL has an aggregation of facilities not found anywhere else in the world; these have national and international recognition for their unique capabilities. The main laboratory consists of 24 low-temperature research coldrooms with a temperature range down to -35°C . Separate facilities include the 73,000-square-foot Ice Engineering Facility (IEF), which houses three special-purpose research areas: a large low-temperature towing tank, a 100-foot-long refrigerated flume for modeling rivers, and a large hydraulic-model room for studying ice impacts on civil works facilities, primarily locks and dams. The 27,000-square-foot Frost Effects Research Facility (FERF) supports full-scale research on the impact of freeze-thaw cycles on pavements, foundations, and utility systems.

3 Executive Summary

Four series of tests were performed on the EMAS cellular concrete to ascertain the system's performance under cold weather conditions.

Large-scale bed cycling

A large-scale EMAS bed was thermally cycled from -20° F to room temperature for 20 cycles over a nine-month period. Qualitative condition assessments were performed during the cycling and quantitative post-cycling punch testing was performed and compared to pre-cycling punch tests. The qualitative assessments found some tape deterioration at the seams and flashing splits at the vents. Nearly all the vents became filled with frost when exposed to the below-freezing temperatures. Visual inspections at the end of cycling found frost buildup in the upper sections of the seams between blocks. The frost did not appear to affect the integrity of the EMAS material.

The quantitative data showed a small but statistically insignificant increase in average block punch strength when the before-cycling and after-cycling punch strengths were compared.

Temperature and humidity cycling

A set of one-cubic-foot EMAS samples was temperature-cycled from -50° F to room temperature and 20% to 100% relative humidity for 20 cycles. A second set was temperature-cycled only and a third set was held at room temperature as a control. Punch tests were performed on the three sets after cycling.

There was no significant difference in the average punch strength values of the three sets of data. The dry-cycled stress/displacement slope was significantly flatter than the other two sample sets.

Seam tape adhesion tests

Two types of seam sealing tape, Tedlar/butyl and silicone, were tested in this study. Five sets of test coupons consisting of two pieces of top material held together with sealing tape, five samples each, were fabricated. Four

sets were temperature-cycled from -50 F to 70 F, with the fifth set held at room temperature as a control. After cycling, the sets were tension-tested at four different temperatures: room temperature, 0° F, -20° F, and -50° F. The control set was tested at room temperature.

The Tedlar/butyl tape showed a significant strength increase with decreasing temperature. It failed at room temperature through delamination between the Tedlar and butyl. At cold temperatures this delamination did not occur and failure was in the Tedlar.

The silicone tape showed only a slight strength increase with decreasing temperature, but at room temperature it was about twice as strong as the Tedlar/butyl. It remained adhered to the top throughout the tensile tests at all temperatures tested.

Top durability tests

Two types of indenters, a steel eyebolt and steel round ball, were dropped onto EMAS blocks at room temperature and -15° F. The drops were from various heights starting close to the block and continuing up until the indenter broke through the top. The indentation volume from the impact was measured for each drop and plotted against the drop kinetic energy.

The eyebolt results showed the top to have a strength increase at -15° F throughout the kinetic energy range of the tests. The round ball results showed no difference between the -15° F and room temperature results for the lower energy ranges and a slight increase in the -15° F strength at the upper kinetic energies.

Overall

Overall the large-scale test showed the EMAS system tolerated the cold cycling well with little change in punch strength. The initial Tedlar/butyl seam tape showed some deterioration during the cycling. The subsequent replacement silicone seam tape underwent only a few thermal cycles but showed no deterioration over those cycles. The material is identical to the side flashing used on the EMAS blocks, which showed no deterioration during the cycling except at some vent protrusions where it had been split. There were a few splits at the vents that had progressed beyond the vent caulking that would be a maintenance point for any installation.

The moisture present in the seams appeared not to have deteriorated the EMAS over the length of this cycling but there was a significant amount of frost found during the cold inspections at the bed teardown.

The EMAS samples tolerated the cold and humidity tests with no significant punch strength change. Generally, both seam tapes performed well in the cold with a tensile strength increase. The block tops also showed a slight puncture strength increase with decreasing temperature.

4 EMAS Description

EMAS is a cellular concrete product that is typically placed at the end of airport runways to form an arrestment bed to replace or supplement Standard Runway End Safety Areas that are not adequate for current safety regulations, as shown in Figure 1. The material is manufactured in 4-ft × 4-ft blocks in 8-, 14- and 20-inch thicknesses with plastic tops and bottoms (Figure 2). There is an open weave scrim molded into the plastic top and brought down over the sides of the block to hold the top in place. It is glued to a similar scrim placed on the plastic bottom before the cellular concrete is added.



Figure 1. EMAS bed at Chicago Midway Airport. (Photo courtesy of ESCO.)



Figure 2. EMAS 4-ft × 4-ft × 20-inch-thick block.

The blocks are adhered to the pavement side by side with a 0.5-inch gap between blocks to form the arrestment bed (Figure 3). The gaps between blocks are covered with a sealing tape and the exterior block edges with a silicone flashing to waterproof the system. This test bed was initially installed with a butyl/Tedlar tape combination as shown in Figure 4.



Figure 3. Side view of EMAS bed being installed for testing at CRREL.



Figure 4. Butyl and tedlar tape being applied to gap between blocks.

After about five months of cycling, a portion of the bed's tape was overlain with a silicone tape that ESCO had switched to as shown in Figure 5. Figure 6 shows the side flashing.



Figure 5. Silicone seam tape applied to gaps between EMAS boards.



Figure 6. Side flashing applied to exposed side of EMAS.

Plastic vents (Figure 7) are inserted between blocks at the exterior edges to promote moisture vapor dissipation from inside the bed.



Figure 7. Plastic vent in vertical part of gap between EMAS blocks. Note the side flashing has not been applied yet to the exposed EMAS edge.

5 Study Rationale and Test Descriptions

An EMAS installation in a cold environment will be exposed to more than just cold temperatures. Past work that CRREL has done in built-up roofing and building systems has shown that moisture condensation and intrusion into insulations and building components can degrade these components over time. Moisture condensation can be accelerated by temperatures cycling from warm temperature where more moisture can be in the air to cold temperatures where it condenses out of the air. Also, if a large amount of moisture is present in a component subjected to freezing, the freeze–thaw process can mechanically break it apart. If the components are susceptible to moisture-induced degradation, then it is important to protect them from moisture intrusion. In an EMAS installation, it is the block top and bottom along with the joint and side sealing tape that provide the majority of the moisture protection to the cellular concrete. Our tests were designed to check these components when subjected to cold cycling as well as the effect of temperature and humidity cycling on the cellular concrete itself.

There were four main components to the cold weather performance testing done at CRREL, as follows:

- Temperature cycling of a large-scale EMAS bed system;
- Vapor and temperature cycling of the cellular concrete;
- Seam tape adhesion tests;
- Top durability tests.

Tests reflected conditions that the EMAS could encounter in a cold environment installation. Although classic material tests *per se* were not desired, it was felt that some were necessary to adequately and economically determine the effect of cold cycling on the system's performance. Where possible, these were performed to reflect the environmental effect on the component as it related to the system, e.g., the top durability test was done with the top on the block rather than as a separate material test on the component alone, as explained later.

Large-scale bed cycling

The large-scale bed cycling was performed in CRREL's Ice Engineering Facility's Research Area. This has a clear span area of 50 ft by 120 ft with a low temperature capability of -20° F. A 44- by 80-ft EMAS bed was installed there with various sensors to monitor temperature and relative humidity (RH) in the gaps between the blocks and temperature under and inside two blocks, as well as ambient conditions. In addition to these measurements, periodic inspections of the bed were performed to document any visible changes. The cooling of the research area is generated by a two-stage, direct-expansion ammonia-based central refrigeration system. The research area is split into four zones with each zone's temperature individually computer-controlled to a tolerance of 1° F to the desired temperature. The internal block temperatures of the two instrumented blocks were continuously monitored and used to decide when to cycle the temperatures as described below. Additional humidity over what was naturally present was not introduced in the experiments. This varied from relatively high in the summer months to relatively low in the winter. Specific values can be found in the Humidity Discussion section below.

Temperature cycling started on June 21, 2007, and ended on March 15, 2008, for a total of 20 cycles. The time scale on the graphs shown in this report are Julian Day in 2007 but modified slightly in 2008 for consecutive days. In other words, the cycling started Julian day 172 and ended Julian day 441. The cycling was briefly suspended from about Julian day 360 to Julian day 390 for equipment maintenance. This hiatus is not included in the data analysis below. At the completion of 20 temperature cycles, selected blocks were pulled from the bed and inspected while the ambient temperature was still below freezing. This allowed us to look for moisture indications and to track its location before thawing when it would migrate as a result of gravity.

Instrumentation

Figure 8 shows the overall EMAS layout with row and column numbers and locations of the temperature thermocouples and dual relative humidity/temperature sensors. Figure 9 is a closer view of the sensor locations with the sensor labels. "RH1" is a combined RH/temperature sensor as were the sensors at the locations named "Vent," which were installed directly behind a vent located in the seam. The temperature sensors labeled F1–F8 were type-T thermocouples with a temperature accuracy of less

than $\pm 1^\circ \text{C}$. The RH/temperature sensors were Precon, HS 2000V models. Precon lists the HS2000V as having a typical $\pm 2\%$ RH accuracy and a $\pm 0.4^\circ \text{C}$ temperature accuracy. More complete specifications on these sensors can be found at http://www.preconusa.com/humidity_moisture_dew_sensors.htm. Figure 10 shows a thermocouple attached below a Precon temp/RH sensor on the side of an EMAS block to monitor the seam temperature and RH.

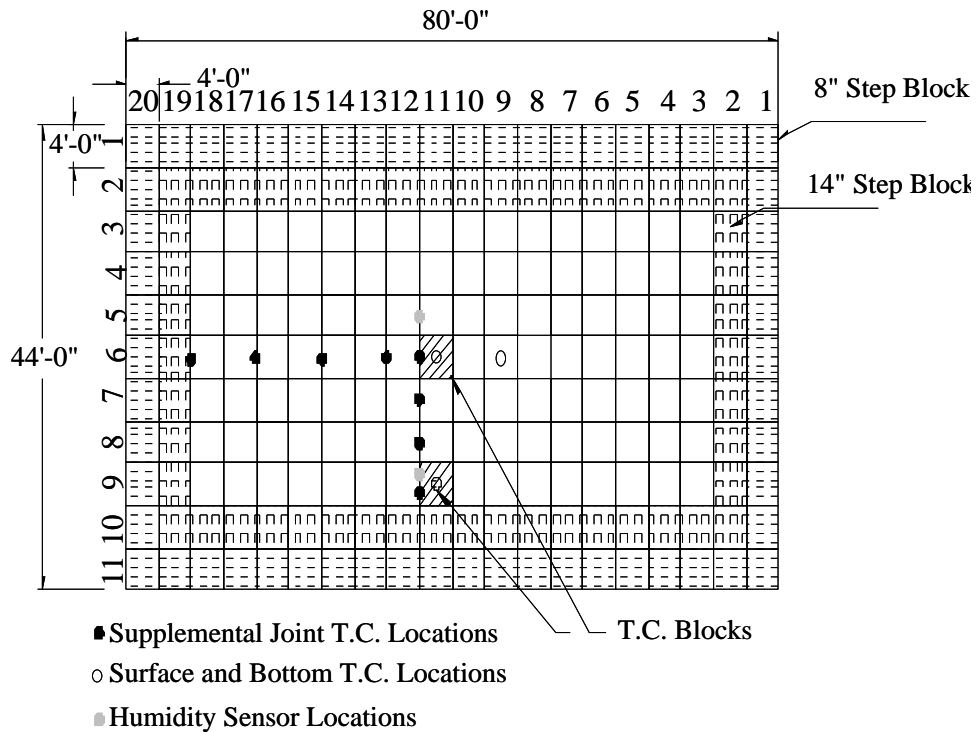
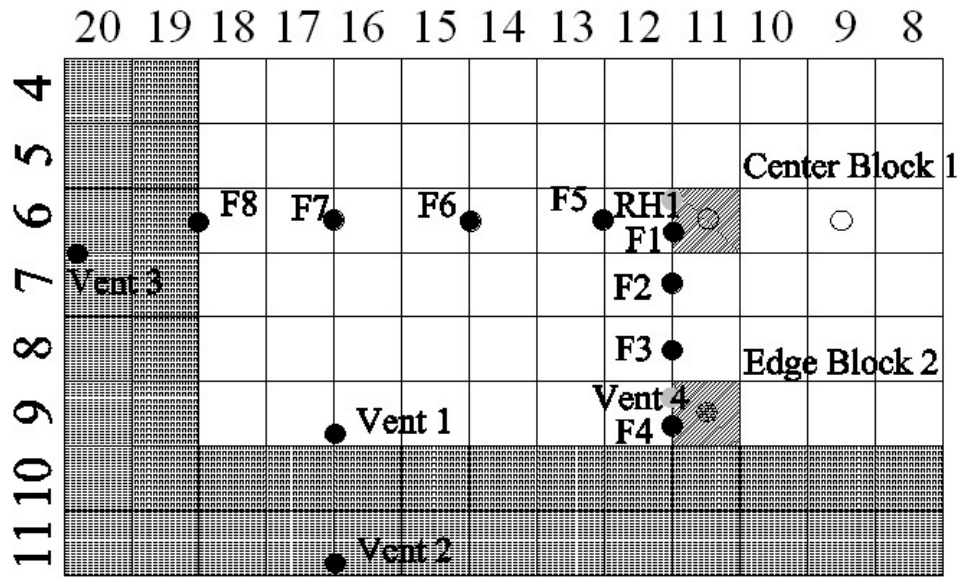


Figure 8. Overall EMAS bed layout with row and column numbers and sensor locations.



Dual Temp and RH sensors		"Fly" Thermocouples (TC)	
Name	Location	Name	Location
RH1	Seam adjacent to center block 1	F1	Row 6, col 11-12
Vent 1	Row 9, col 16-17 at 20" block	F2	Row 7, col 11-12
Vent 2	Row 11, col 16-17 at 8" block	F3	Row 8, col 11-12
Vent 3	Row 6-7, col 20 at 8" block	F4	Row 9, col 11-12
Vent 4	Row 9, col 11-12 at 20" block	F5	Row 6, col 12-13
		F6	Row 6, col 14-15
		F7	Row 6, col 16-17
		F8	Row 6, col 18-19

Figure 9. Detail view of the EMAS bed sensor layout with sensor labels.



Figure 10. Precon temperature/RH sensor and a thermocouple (red tip) mounted on the side of a block.

Two blocks, called Center Block 1 and Edge Block 2, were instrumented with thermocouples at three levels to monitor internal temperatures as shown in Figure 11. The sensors were automatically read by a Campbell CR 10X datalogger at one sample every fifteen minutes (Figure 12).

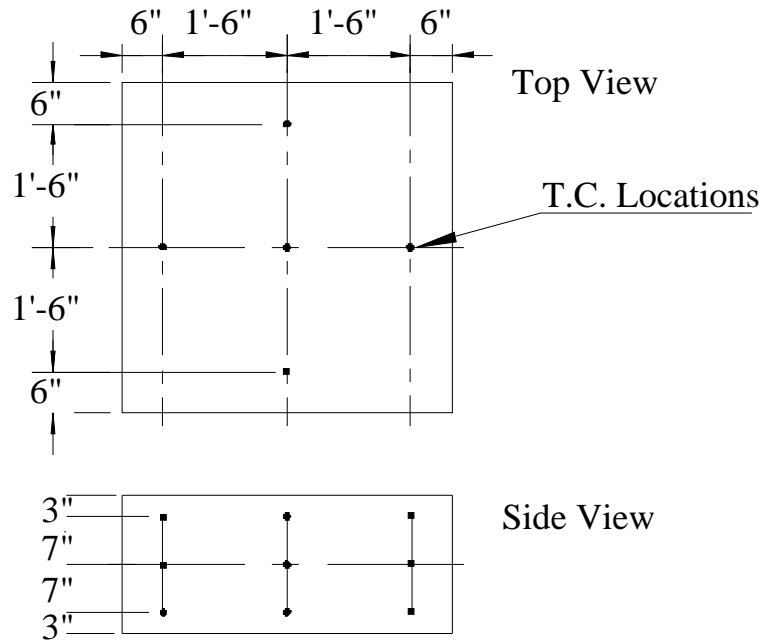


Figure 11. Thermocouple layout used in instrumented center and edge blocks.



Figure 12. Campbell datalogging system.

Temperature discussion

The cellular concrete in the EMAS has a relatively high thermal resistance, which makes heating and cooling the interior of the block a slow process. There was a temperature difference between the bottom of the block and the ambient room temperature above the EMAS as there would be in a bed installed at a runway. However, the surface temperature of an installed EMAS bed would probably be much higher than those achieved during our tests due to solar heating. The economics of the study required a temperature criterion that was achievable within the projected budget. It was decided to cycle the ambient temperature from -20°F up to room temperature, which varied generally from about 55°F in the winter to 85°F in the summer. The temperatures were held until the block center reached $+35^{\circ}\text{F}$ on the warm cycle and 25°F on the cold cycle. A total of 20 cycles were completed with a somewhat longer period at -20°F at the end of the 20 cycles. This temperature criteria produced a temperature difference during cooling from about 42°F at the block bottom to -20°F at the block top surface with mid-level (10 inches deep) block temperatures cycling between 25°F and $+35^{\circ}\text{F}$. To illustrate the temperature variation, Figure 13 shows typical ambient, under-the-block, and mid-level temperatures from the three center thermocouples in Center Block 1 (20 inches thick) for some representative cycles from Julian days 300 to 330.

Seam temperatures are shown for the same days from thermocouples F1–F4 in Figure 14 and F5–F8 in Figure 15.

Seam temperatures measured by the RH/temperature sensors are shown in Figure 16.

Table 1 lists the temperature range and mean for each center thermocouple from Center Block 1 and Edge Block 2 for all the cycles performed. The Edge Block temperatures were slightly cooler than the Center Block. Table 2 shows the range and mean for all the seam temperatures to the nearest 0.5°F .

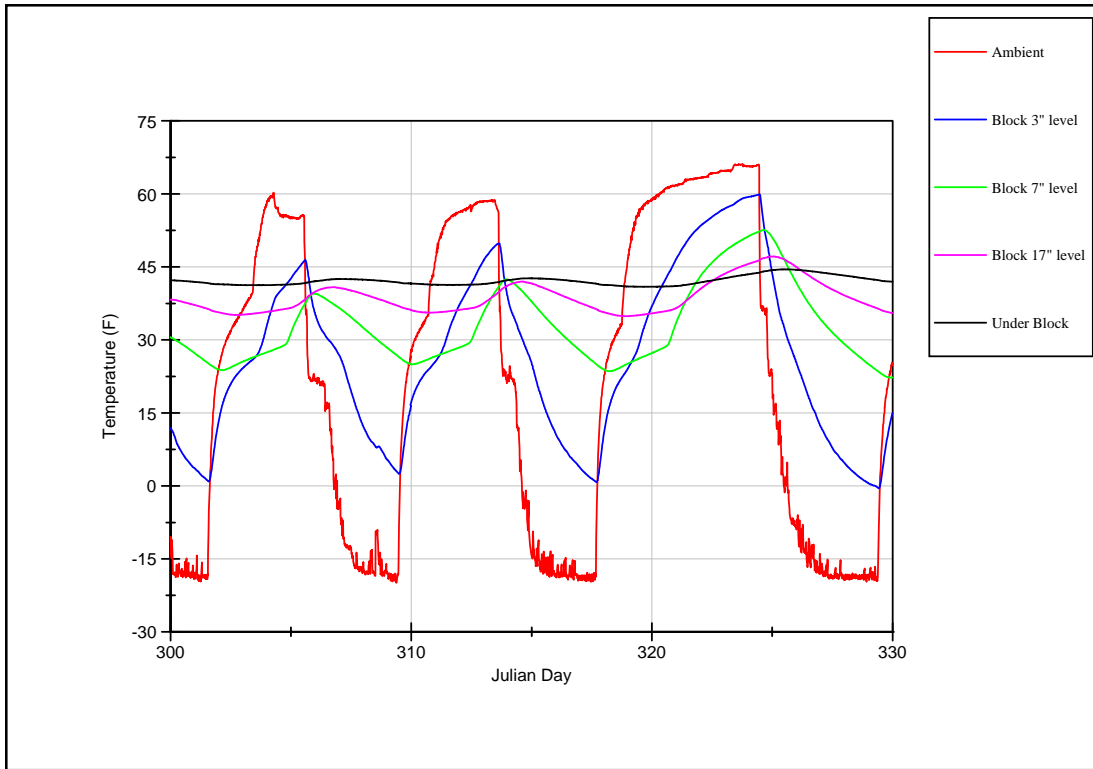


Figure 13. Ambient, in-block, and beneath-block temperatures for Julian days 300–330.

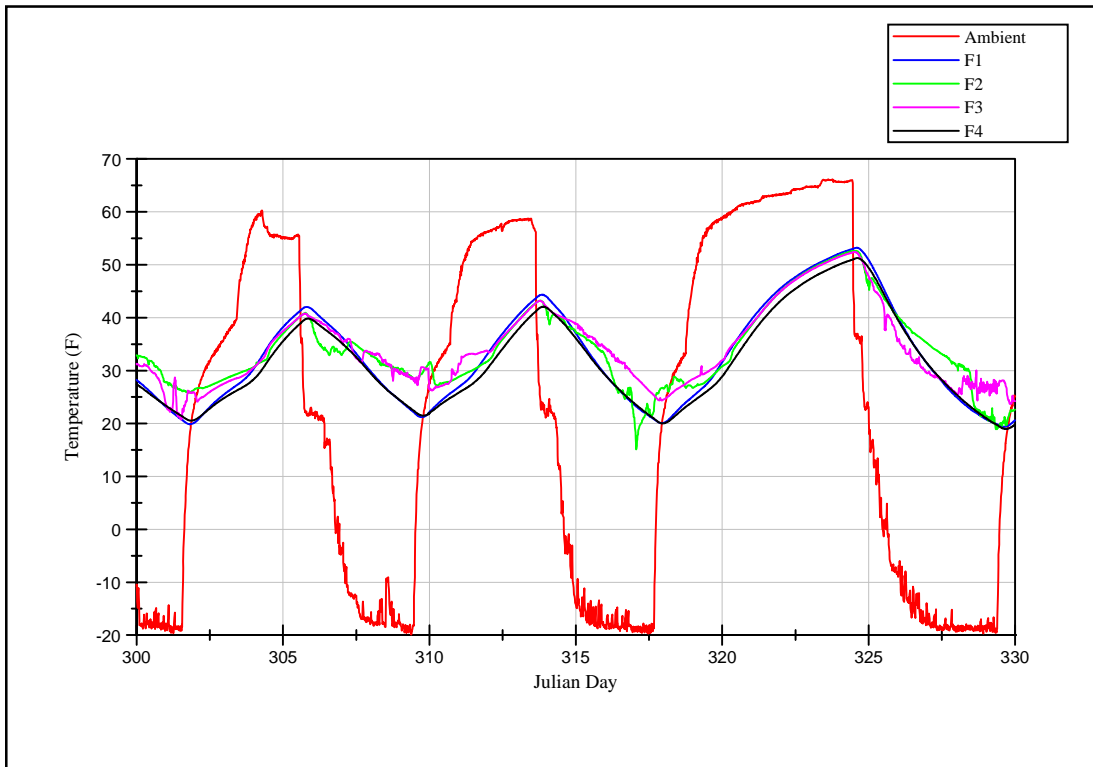


Figure 14. Seam temperatures from thermocouples F1–F4, Julian days 300–330.

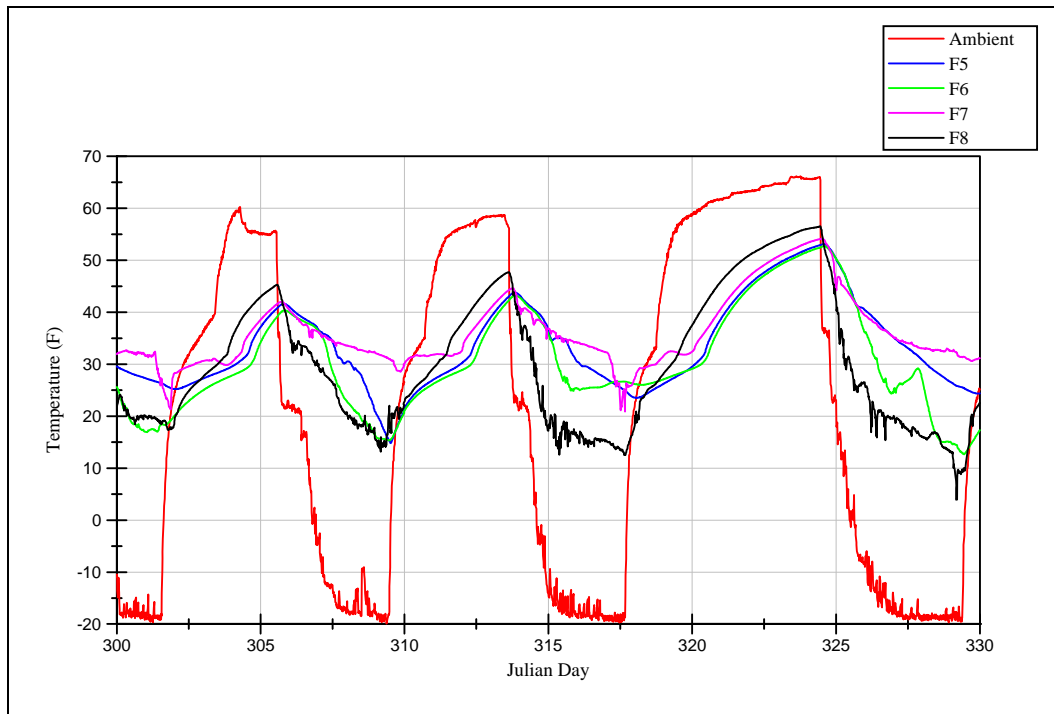


Figure 15. Seam temperatures from thermocouples F5-F8 for Julian days 300-330.

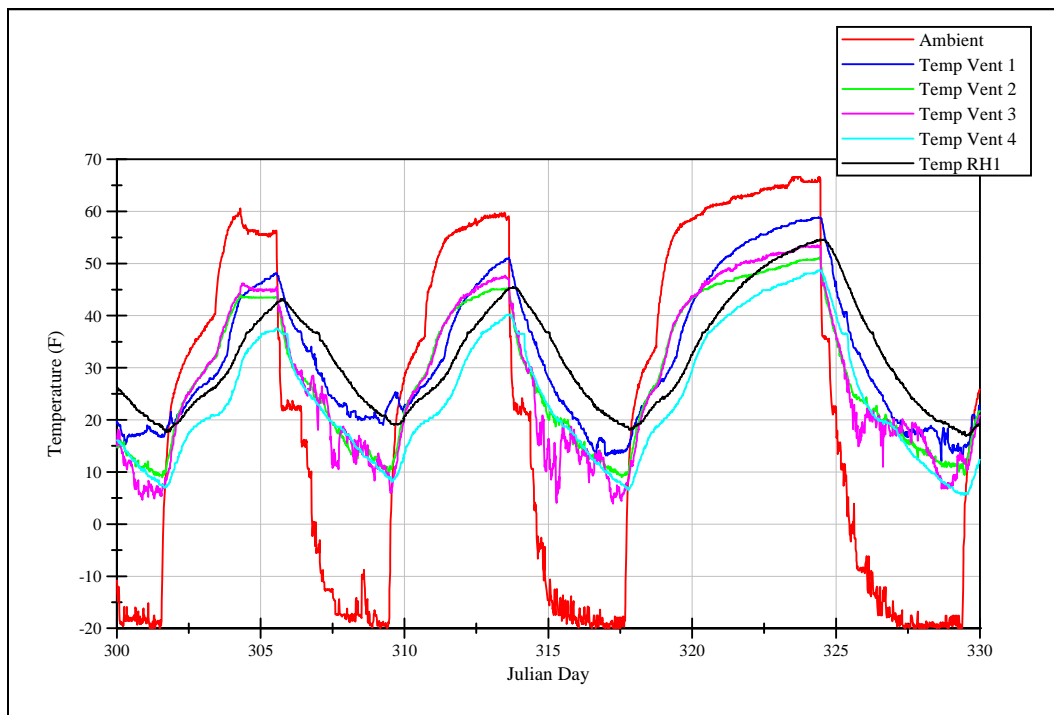


Figure 16. Temperatures measured by the Precon sensors at four vent locations and an interior seam, Julian days 300-330.

Table 1. Temperature ranges and means throughout the block thickness from the center and edge blocks, Julian days 300–330.

Location	Center Block 1			Edge Block 2		
	Low to High (°F)	Range (°F)	Mean (°F)	Low to High (°F)	Range (°F)	Mean (°F)
Ambient	-20.0 to 74.1	94.1	16.7	-20.0 to 74.1	94.1	16.7
3-inch depth	-6.4 to 74.5	80.9	23.5	-4.9 to 74.2	79.1	23.5
10-inch depth	11.5 to 72.6	61.1	33.2	10.2 to 72.6	62.4	31.3
17-inch depth	27.6 to 71.2	43.6	41.9	27.2 to 71.0	43.8	40.2
Under	36.5 to 70.4	33.9	46.4	34.3 to 70.3	36.0	43.8

Table 2. Range and mean seam temperatures for all cycles.

Location	Low to High Temperatures (°F)	Range (°F)	Mean (°F)
F1	10.7 to 73.2	62.5	33.1
F2	7.9 to 72.4	64.5	35.2
F3	15.1 to 72.8	57.7	35.9
F4	11.2 to 72.8	61.7	32.2
F5	9.8 to 72.9	63.1	34.7
F6	3.7 to 72.3	68.6	32.8
F7	14.4 to 72.9	58.5	35.8
F8	2.8 to 73.3	70.5	29.4
Vent 1	6.4 to 75	68.6	31.4
Vent 2	2.8 to 72.9	70.1	27.0
Vent 3	-5.8 to 74.1	79.9	26.7
Vent 4	1.2 to 74.4	73.2	24.7
RH1	8.6 to 73.9	65.3	32.1

There are a few trends evident in the seam temperature data.

The four vent mean temperatures average out to 27.5° F, which is colder than the average mean temperature of all the other seam thermocouples (F1–F8) at 33.6° F. The vent temperature measurements were taken directly behind the vent and slightly higher than the seam thermocouples, which were placed halfway down the block, as shown in Figure 17.



Figure 17. EMAS block being installed showing locations of thermocouple (at left) and Precon temperature/relative humidity sensor nearer where the vent eventually will be installed.

Thermocouples F4 and F8 in the exterior seams next to the 14-inch step blocks average 30.8°F . The remaining interior thermocouples F1–F3 and F5–F7 average 34.6°F . These trends appear to show the effect of a warmer interior bed versus the exterior, more exposed, seams at the step blocks.

The temperatures of the two lower vents, Vent 2 and Vent 3, placed in the bottom 8-inch-thick blocks were examined against Vents 1 and 4 placed in the higher, 20-inch blocks to see if there was a temperature stratification evident. Vents 2 and 3 average 26.9°F with their means only 0.3°F apart. Vent 1's mean is 31.4°F and Vent 4's is 24.7°F , a 6.7°F difference, but together they average 28.1°F , slightly higher than the two lower vents. The wide temperature difference between Vent 1 and Vent 4 is unexplained. Thermocouple F4 in the same seam as Vent 4, but lower and toward the block center, has a mean of 32.2°F , similar to Vent 1's mean of 31.4°F . Vent 4 has the lowest mean seam or vent temperature of all the data.

The interior seam temperatures along column 11–12 from F1–F3 average 34.7°F . The interior seam temperatures along row 6, F5–F7, average 34.4°F , showing consistency between all the interior seam temperatures.

Humidity discussion

Relative humidity is vapor pressure divided by saturation vapor pressure times 100%. The saturation vapor pressure of water is temperature de-

pendant with a higher temperature having a higher saturation vapor pressure. At saturation vapor pressure, air has a RH of 100%, and any increase in water vapor pressure or decrease in temperature will cause condensation. Figure 18 is a graph of ambient temperature and relative humidity over the EMAS for Julian days 202.5 to 252.5. The RH data fluctuated enough to make interpretation of the graphs difficult so the data has been smoothed for clarity. It shows the expected trend (with no water vapor added or removed) of increasing RH with decreasing temperature and conversely decreasing RH with increasing ambient temperature.

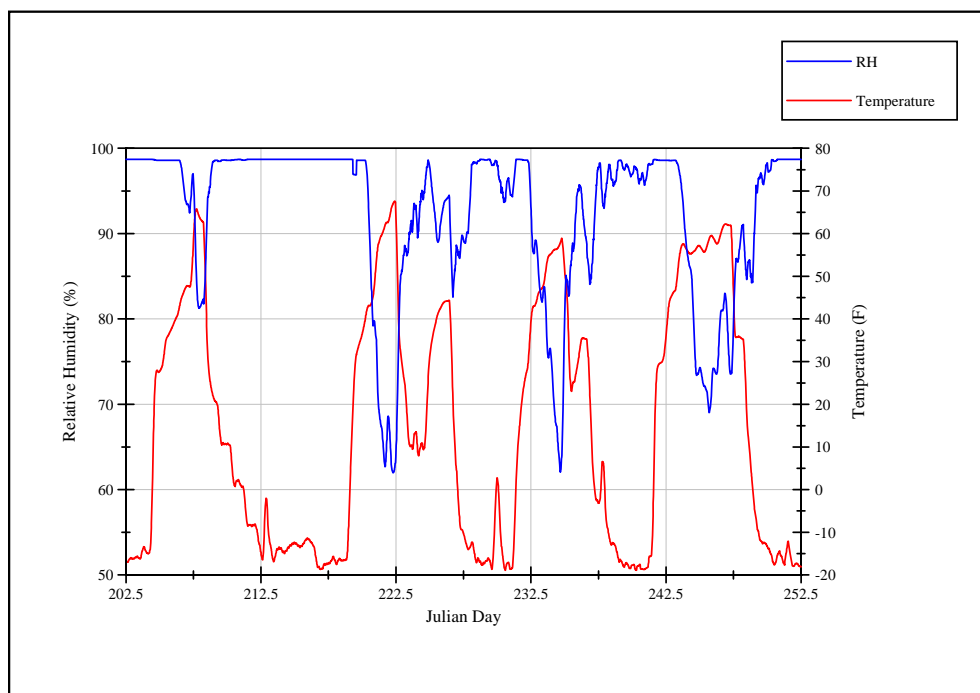


Figure 18. Ambient temperature and RH over EMAS bed during cycling.

Figure 19 shows the initial RH from the start of cycling to Julian day 207.5 and Figure 20 presents the temperatures for the same time period measured by the same temperature/RH sensors. From the start of cycling on Julian Day 172.5, the RH behind Vent 1 quickly rose from about 85% RH to essentially 99% RH by day 177.5, where it remained for the rest of the cycling. The RH at locations Vent 4 and RH1 started at about 88% and took about 30 days to day 202.5 to rise to 99% RH, where Vent 4 remained for the rest of the cycling while RH1 fluctuated between 99% and 82% for the rest of the cycling. The RHs behind Vents 2 and 3 were varying around 60% to 70% for the same time, until they also rose to about 98% by day 205. However, the RH at these vents fluctuated throughout the cycling as shown in Figure 21. The ambient RH started at about 60% and reached

99% at about Julian day 190. Figure 20 shows the ambient temperature was slowly dropping from the start of cycling to about Julian day 197, where it leveled off at -20° F. The RH behind Vent 2 and Vent 3 initially remained substantially lower than at the other locations, even though the temperatures at the two vents were similar to Vent 4 and colder than at Vent 1 and RH1. It was almost Julian day 206 before the RH at Vents 2 and 3 increased rapidly to nearly 100%. This coincided with the beginning of a warming portion of the cycle. Vents 2 and 3 are physically the lowest vents in the bed.

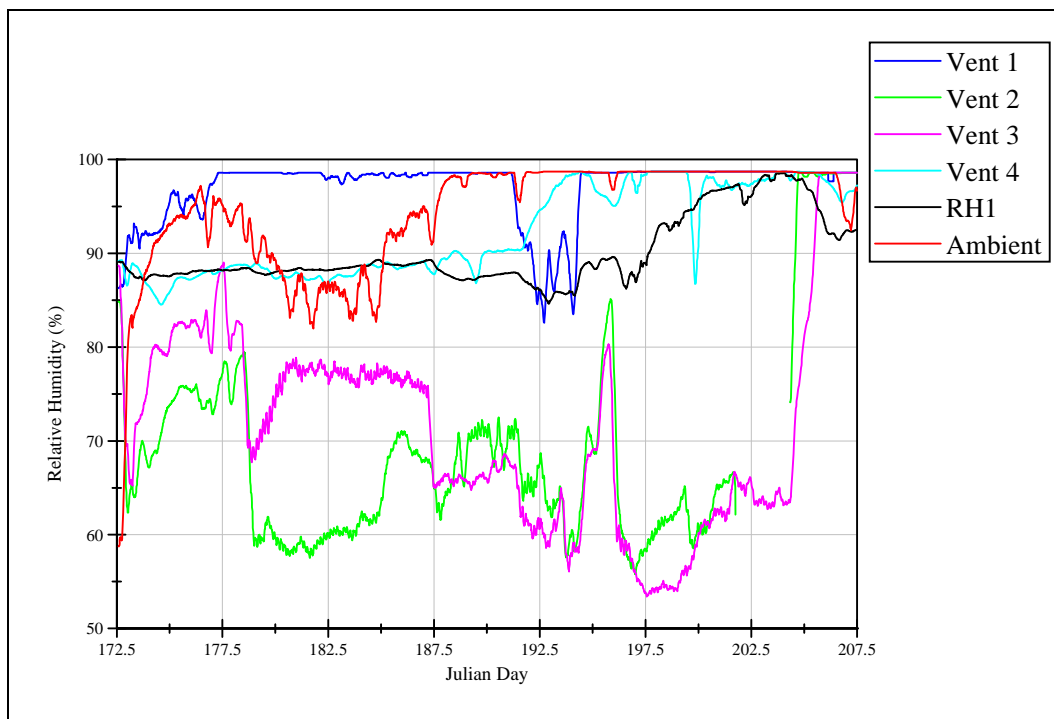


Figure 19. Smoothed relative humidity at the start of cycling.

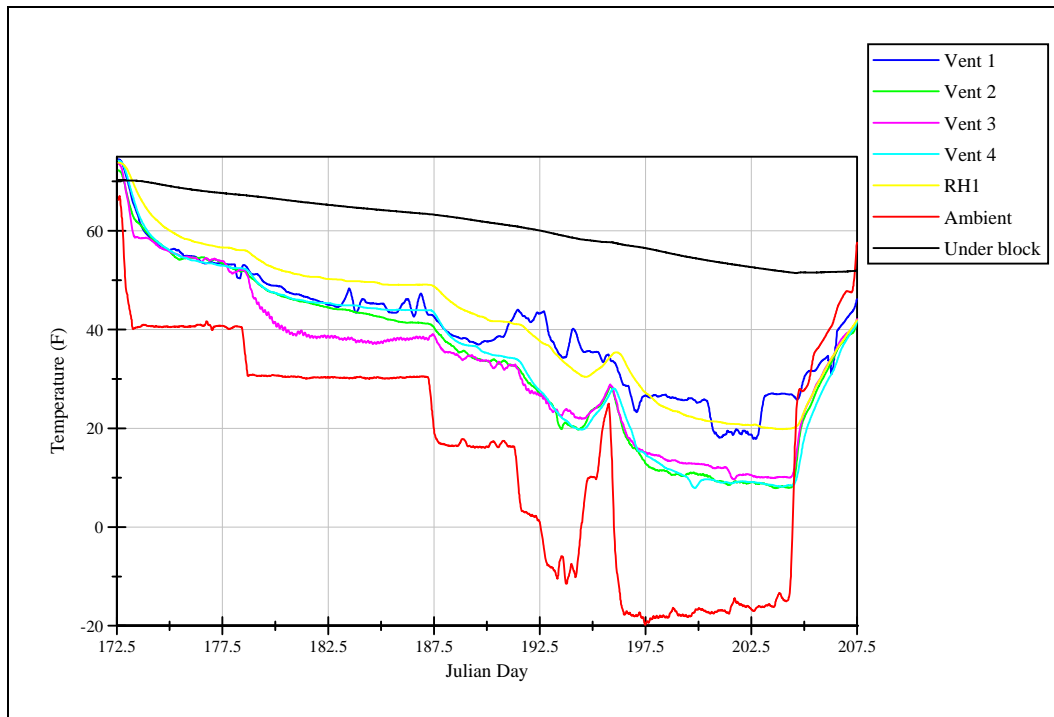


Figure 20. Temperatures measured by the temp/RH sensors Vent 1–Vent 4, RH1 and under a block at the beginning of cycling.

Figure 21 illustrates some typical seam RH trends during cycling with smoothed data from the five seam RH sensors for Julian days 300–330. It shows the RH change was most active behind the lower Vents 2 and 3 with a little change noticeable in RH1, located in an interior seam. Vents 1 and 4 remain pegged at nearly 100% relative humidity. Figure 22 shows the temperatures from the same sensors.

In Figures 21 and 22, it can be seen that the temperature and RH cycles do not alternate but almost coincide with a slight shift. The lowest RH comes just before the lowest temperatures are reached.

Table 3 lists the mean and range RHs from the five RH sensors for all the cycling. The table shows the relative humidity in the seams was high overall, with the highest range and lowest mean values from the lower Vents 2 and 3.

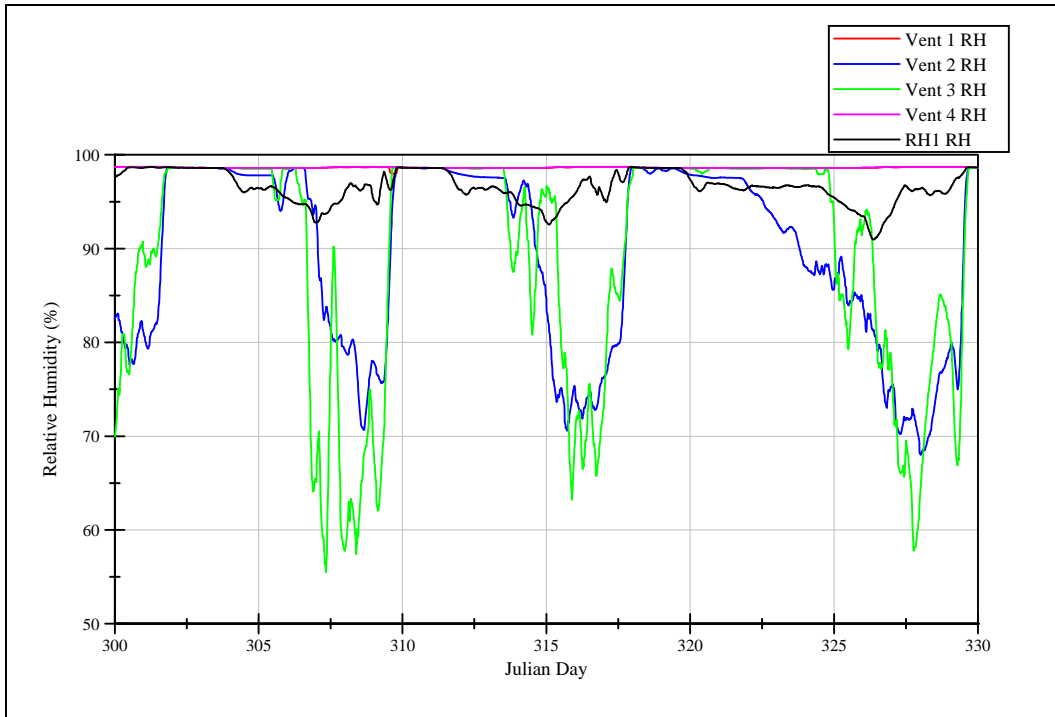


Figure 21. Smoothed relative humidity data, Julian days 300–330.

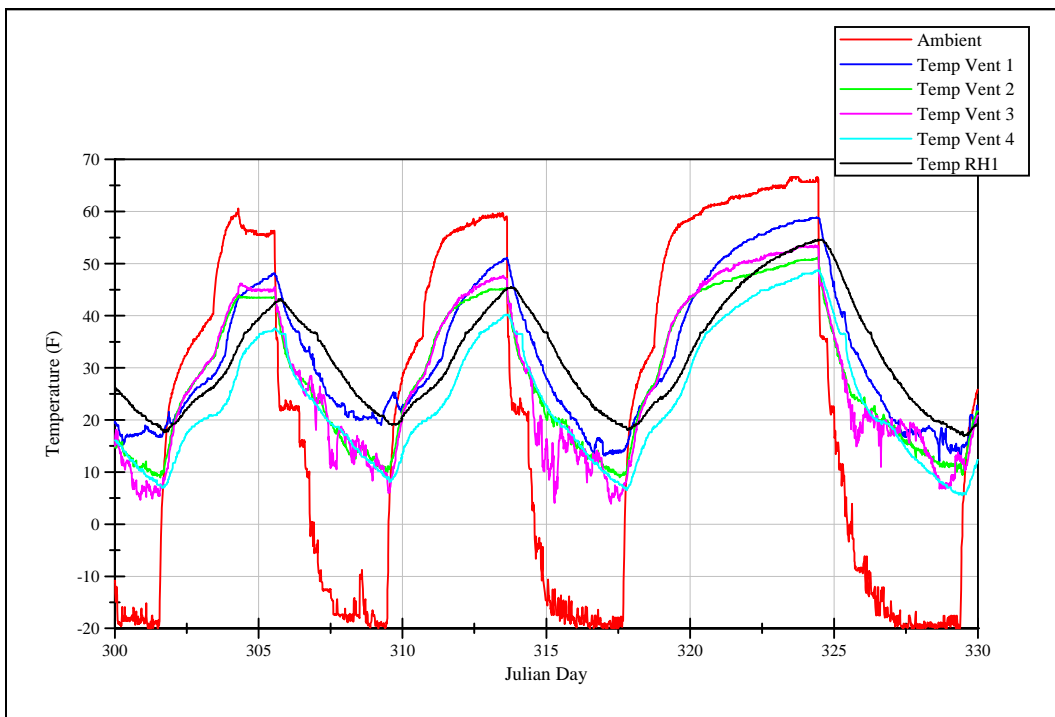


Figure 22. Five seam temperatures with ambient for Julian days 300–330.

Table 3. Relative humidity from all the RH sensors for all cycles.

Location	Low to High Relative Humidity (%)	Range (%)	Mean (%)
Vent 1	75.4 to 98.7	23.3	98.3
Vent 2	43.7 to 98.7	55.0	84.9
Vent 3	32.2 to 98.7	66.5	86.0
Vent 4	81.7 to 98.7	17.0	97.6
RH1	82.1 to 98.7	16.6	95.2

Cold inspections

At the end of the cold cycling, several blocks were removed from the bed and inspected while the ambient temperature was still below freezing. This cold “forensics” allowed us to literally freeze any moisture that might be present in place to help explain the humidity data. During the cold forensics, several blocks were removed from Row 5 starting at Column 20 and continuing into the bed until Column 15. Small amounts of frost were found in the upper section of the seam between the lowest 8-inch-thick blocks in Column 20 as shown in Figure 23. More frost was found under the flashing in the seam between Column 20 and Column 19, where the 8-inch block met the 14-inch block as shown in Figure 24. The seams between the 14-inch-thick blocks (Column 19) generally had more frost than what was found between the 8-inch-thick blocks (Figure 25). The seam between the 14-inch- and 20-inch-thick blocks had more frost than the seam between the 8-inch- and 14-inch-thick blocks, as shown in Figure 26. Continuing into the bed, the seams between the 20-inch blocks had frost along most of their length down to variable depths along the block sides. Figure 27 shows a typical pattern for the frost distribution on the sides of the blocks. The frost pattern on the sides generally was deeper in the middle of the block, arching upward toward the sides until it would sometimes increase at the corners and other times decrease, as shown in Figures 28 and 29. In the bed interior, when viewed from above, the frost in the seams generally appeared thicker at the block corner intersections (Figure 30).

The frost patterns discovered during the forensics are consistent with the RH data above. The Precon temperature/RH sensors were mounted either in the middle of the block side (RH1) or at the upper corner near a vent. The upper sections of the block were where the frost was heaviest, with the largest amount of moisture coming in the interior and less amounts at the lower step blocks. The middle of the block side is also where the moisture

generally extended down the block side the farthest. The RH data recorded above indicates a high RH in upper blocks starting shortly after the temperature cycling began, with the lower vent RH readings still generally high, but showing some fluctuation.

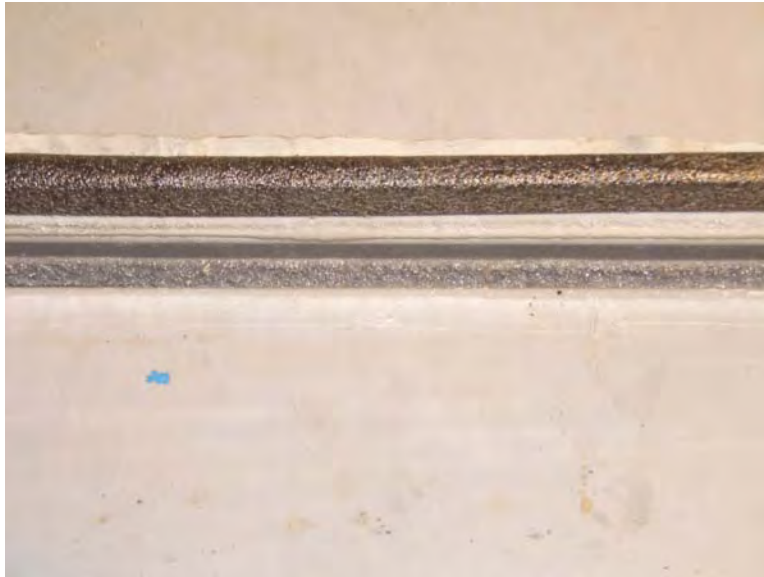


Figure 23. Small amount of frost along underside of sealing tape, row 5, column 20.



Figure 24. Frost where the 8-inch and 14-inch blocks meet.



Figure 25. Slightly more frost between 14-inch-thick blocks in column 19 than found in column 20.



Figure 26. Frost between 14-inch- and 20-inch-thick blocks.



Figure 27. Typical frost pattern on the side of a block.



Figure 28. Frost distribution shows an increase at the corners.



Figure 29. Decreasing frost at some corners.



Figure 30. Thicker frost at the intersection of four blocks.

Nearly all the vents showed frost buildup during the cold portion of the cycling. Figure 31 shows a vent from the lowest 8-inch-thick block. The material stuck on the side of the vent is silicone flashing and marks how far the vent protruded from the block. Figure 32 shows the vent from the second level of step blocks. Note that frost extends the entire length of the vents.



Figure 31. Frost in a vent from the first level of 8-inch-thick blocks.



Figure 32. Frost in the second-level vents.

Qualitative block inspections

A block top was removed during the cold forensics to inspect the condition of the block beneath it. Figure 33 shows the underside of the top with some frost traces visible. The block was dug into with a portion removed as shown in Figure 34. The concrete appeared to be competent with a normal consistency similar to what is found in new blocks, and the cut face profile didn't show any signs of deterioration or voids other than what was caused by the sample removal.



Figure 33. Underside of block top with frost traces.



Figure 34. Sample removed from material directly under the block top.

A similar process was performed on an interior block directly behind where there had been surface frost in the seam as shown in Figure 35. Again the block consistency was normal with no signs of moisture deterioration behind the frost.



Figure 35. Sample cutout from a block side that had surface frost on it. The darker areas are from glue used to hold a scrim material that fastens the plastic block top to the plastic bottom.

Qualitative system inspections

Visual inspections of the EMAS bed were made periodically throughout the temperature cycling. Overall, the bed appeared to perform well with some points listed below.

Vents

As mentioned above, the vents showed frost buildup during the below-freezing temperatures. This was severe enough in a large number of vents to completely plug the vent, as shown in Figures 36 and 37.

Seam tape

About three months into the cycling, several areas of the Tedlar/butyl seam tape showed signs of distress. It appeared to be shrinking and in some cases splitting, as shown in Figure 38a, b, and c. ESCO has since replaced this tape with an all-silicone tape made of the same material as their side flashing that is applied with a silicone adhesive. A section of the EMAS was retrofitted with this tape on 19 November 2007. The new tape went through eight temperature cycles and showed no signs of deterioration from that number of cycles.



Figure 36. Vent frosting completely plugging the vent.



Figure 37. Front view of vent shown in Figure 36 with frost plugging holes.

Sealant at vents

The most prevalent issue noted was the sealant around the vents. After several cycles, either the flashing at the vents started to tear, as shown in Figure 39, or the sealant at the vents started to pull away from the flashing (Figures 40 and 41). These openings could provide a direct moisture path into the seams.



Figure 38 a, b and c. Tedlar/butyl tape showing some splitting and shrinkage.



Figure 39. Flashing tearing above vent.



Figure 40. Vent sealant pulling away from flashing.

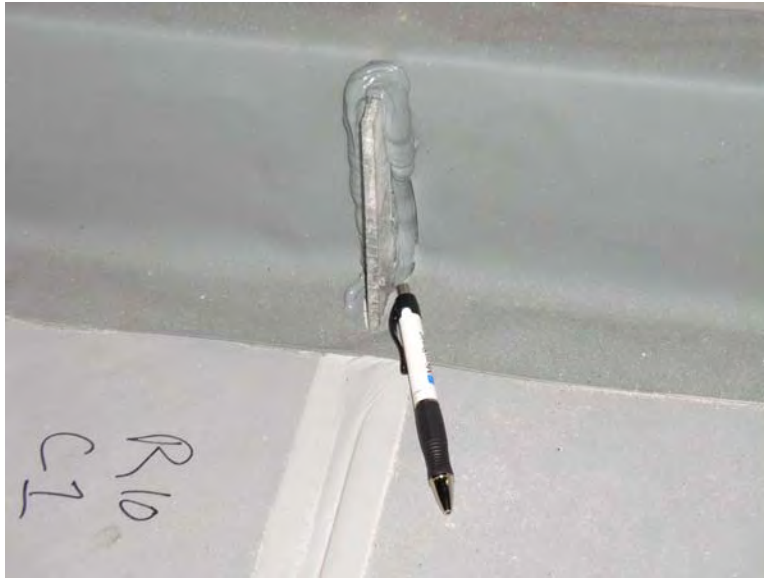


Figure 41. Sealant at vent pulling from flashing.

Quantitative block punch data

To ascertain whether there was any effect from temperature cycling on block strength, block punch tests were performed on 14 blocks before and after temperature cycling. The pre-cycling punch tests were performed at ESCO on the newly manufactured blocks before the tops were installed. Those blocks were then blindly placed into the test bed and tested at CRREL at the completion of the temperature cycling.

Punch procedure

A CRREL Punch Tester (CPT) was designed and fabricated at CRREL to mimic the ESCO punch testing machine. The CPT has a raised floor to hold the EMAS block and a sliding carriage to position the punch head anywhere over the block. Once an EMAS block is set onto the raised floor of the CPT it does not have to be moved again until the punch tests are completed. Several beta blocks were tested at CRREL, with the data sent to ESCO where they verified that our results matched theirs, thus ensuring the before and after punch tests would reflect material changes and not procedure differences. Figure 42 shows the CPT with a block being tested.

Each block except one had two punches done by ESCO and two by CRREL in the same relative block positions to avoid strength differences caused by cure location. Figure 43 shows the general punch locations in the block. The punch tests were performed with a 2-inch-diameter punch head at a rate of approximately 1 inch/second on blocks without the plastic top.



Figure 42. CRREL Punch Tester with an EMAS block in place.

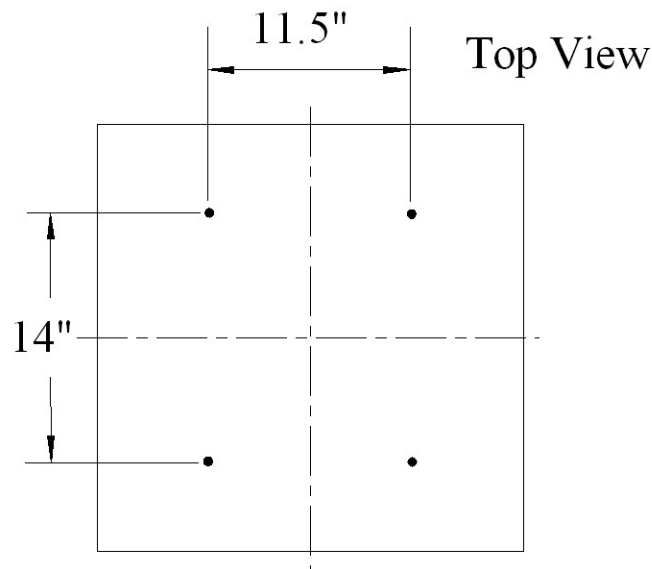


Figure 43. Top view of EMAS block showing punch test locations.

Punch test discussion

Figure 44 is a typical stress versus displacement curve from the punch tests. The displacement is expressed as a fraction of the block depth following a convention used by ESCO. The stress rises steeply initially as the punch first enters the block then levels out at about 0.1 displacement fraction, after which it rises at a constant rate to about 0.7 displacement fraction. Above 0.7 displacement fraction, the punch head is too close to the block bottom and the stress is affected by the material that has accumulated beneath the punch head. The portion of the data between 0.1 and 0.7

displacement fraction and a linear fit curve between the same displacements was used to obtain the data below.

Four metrics were used to analyze the difference between the pre- and post-cycled data:

- The slope of the linear fit curve.
- The average maximum overall pressure. This is the average of the highest stress values from the curves in the above range. The highest stress usually, but not always, occurred at 0.7 displacement fraction.
- The maximum linear pressure value. This is the average of the highest stress values from the linear fit curves. It occurred at 0.7 displacement fraction.
- The 35% displacement stress value. It is the average of the stress taken from the linear fit at 0.35 displacement fraction.

Initially it was thought the linear stress value would be more representative of the material stress by avoiding the effect of scatter in the overall stress data. Table 4 lists the pre- and post-cycling punch data. Figures 45–48 are graphs of the average 35% displacement pressure, average overall maximum pressure, average linear maximum pressure, and average slope with their standard deviations.

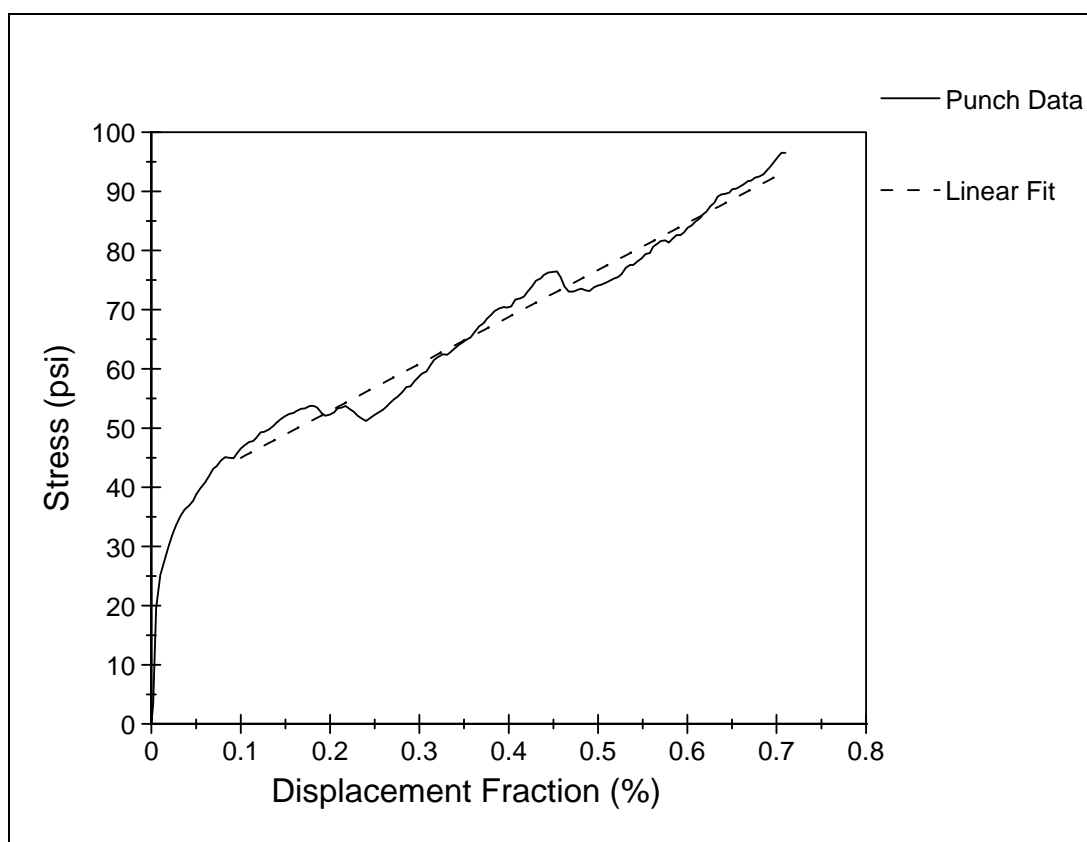


Figure 44. Typical stress versus displacement fraction curve from the block punch data.

Table 4. Pre- and post-cycling stress and slope values.

Test	Average 35% Displacement Pressure	35% Pressure Std. Dev.	Average Max Overall Pressure (psi)	Overall Pressure Std. Dev.	Average Max Linear Pressure (psi)	Linear Press. Std. Dev.	Max Slope (psi/disp. fraction)	Min Slope (psi/disp. fraction)	Average Slope (psi/disp. fraction)	Slope Std. Dev.
Pre	49.5	8.9	61.9	11.9	58.5	10.8	37.2	4.6	25.8	10.3
Post	50.4	8.7	75.2	11.0	72.0	11.7	115.2	25.6	61.9	18.6

The data show the average overall pressure increased about 13.3 psi from the pre-cycle values, which is barely outside their standard deviation of 11 to 11.9 psi. The average linear pressure increased a similar 13.5 psi on a standard deviation of 10.8 to 11.7 psi, and the 35% pressure showed essentially no change. The average slope values showed the most change of 36.1 psi/displacement fraction with standard deviations from 10.3 to 18.6 psi/displacement fraction. The slope values show the rate of increase of the pressure between 0.1 and 0.7 displacement fraction, and it seems that although the maximum pressure values showed a very slight increase after cycling, the average rate of the increase was higher, perhaps indicating a

slight stiffening or slight brittle increase of the material. In either case, the changes in punch stress between pre- and post-cycling do not appear significant.

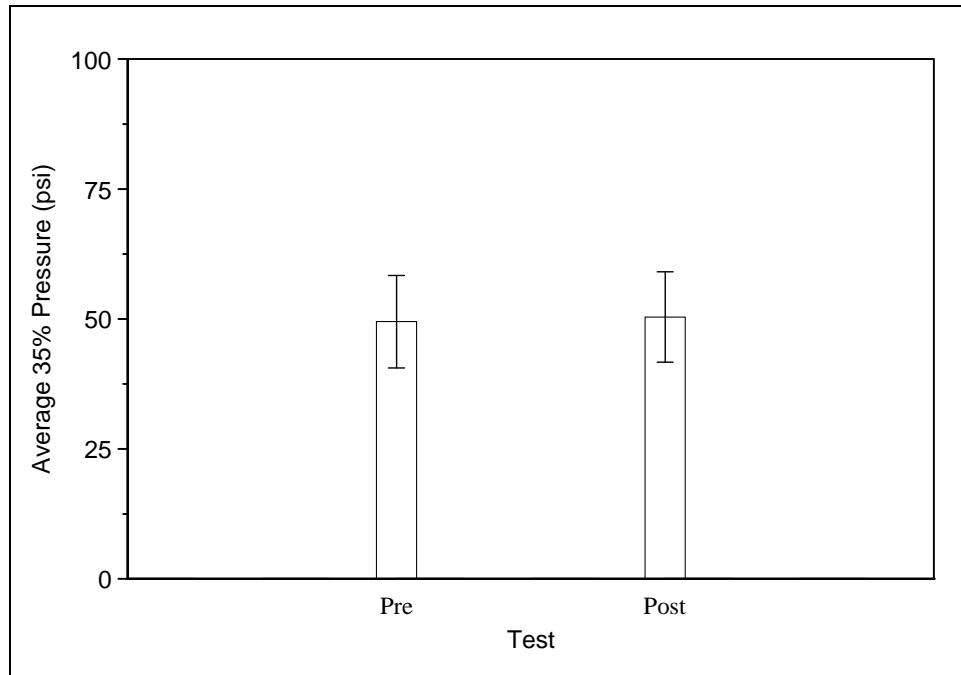


Figure 45. Average stress at 35% displacement fraction pre- and post-thermal cycling comparison.

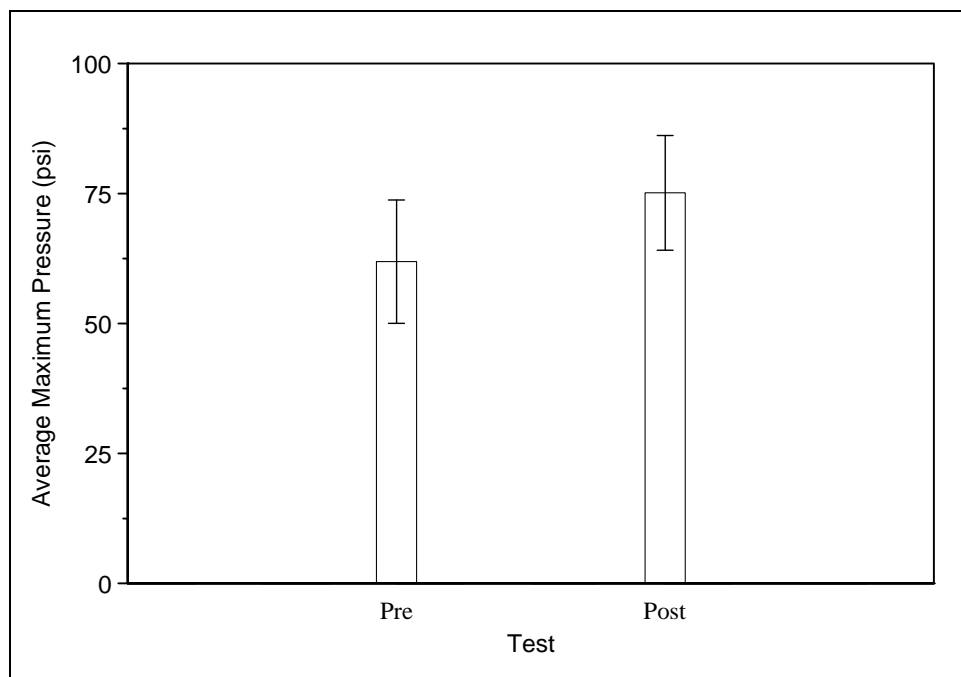


Figure 46. Average maximum stress pre- and post-thermal cycling comparison.

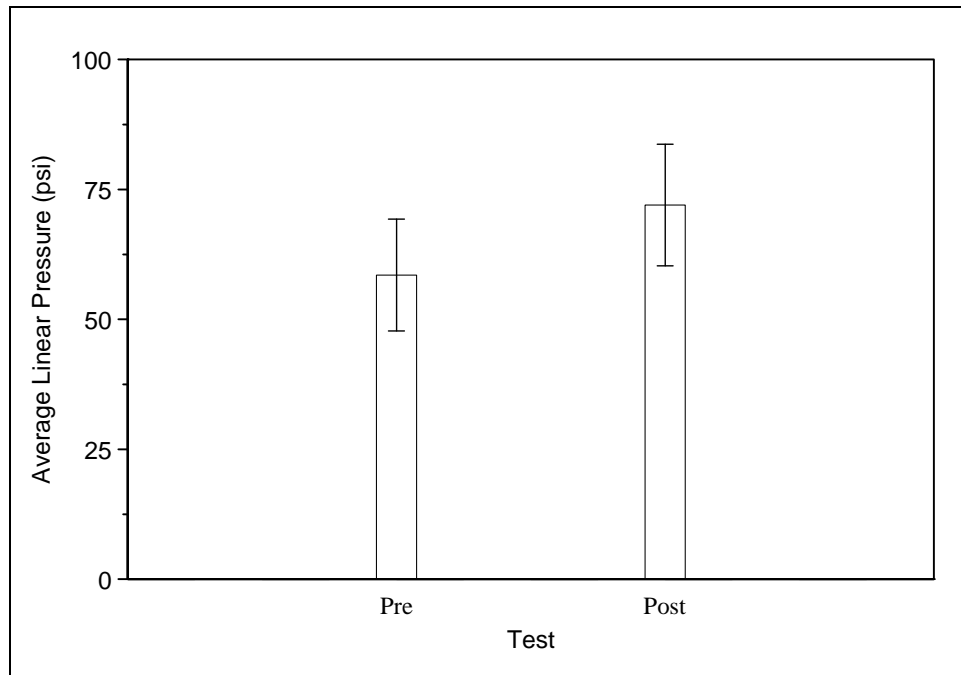


Figure 47. Average maximum linear stress pre- and post-thermal cycling comparison.

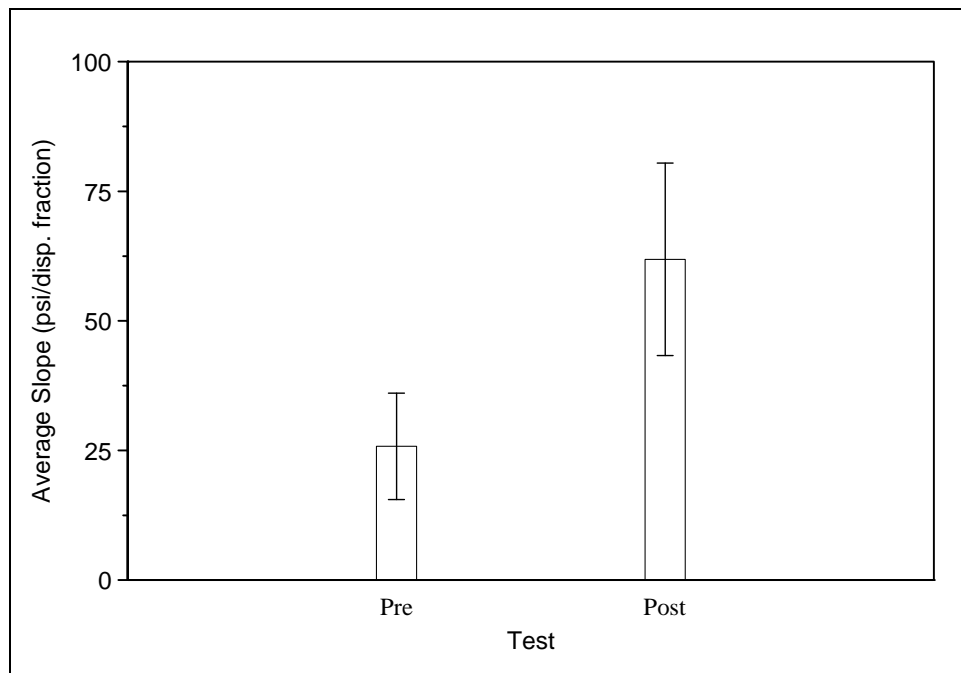


Figure 48. Average linear fit slope pre- and post-thermal cycling comparison.

Temperature and humidity cycling tests

An EMAS installation will probably be exposed to water vapor as the vapor intrudes into the seam voids from moist ground or through the vents from humid air. Also, the cellular concrete material will initially vent moisture

as it cures for some time after manufacture. A modified vapor porosity test was performed to see if there was an effect on the EMAS from a combined high vapor environment and temperature cycling. The tests were designed so as not to force vapor into the material, but to expose it to vapor under conditions that could be found during an installed life.

Three sets of four 1-cubic-foot samples were used in this test. One set was temperature- and humidity-cycled for 20 cycles in a CRREL environmental box (shown in Figure 49). The temperatures ranged from -50° F to room temperature (50° F to 75° F) and the relative humidity ranged from 20% to 100%. Figure 50 shows a typical portion of the temperature and humidity record. Another set of samples was dry-cycled under the same temperature range listed above, and the third set consisted of control samples maintained at room temperature and not subjected to any temperature or humidity cycling.

Each sample set was punch-tested with the stress and slope recorded using a procedure similar to the large-scale pre- and post-cycling tests above.



Figure 49. CRREL temperature chamber.

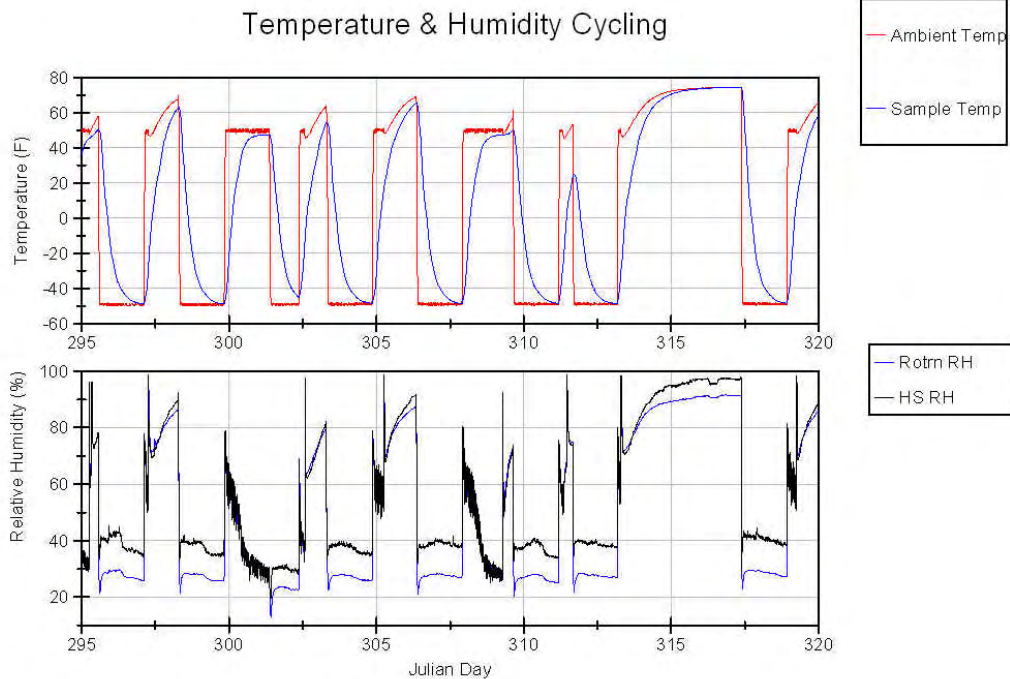


Figure 50. Temperature and humidity example. The temperature graph shows the ambient and internal sample temperature. The bottom humidity graph shows readings from two separate humidity sensors.

Humidity test discussion

Figure 51 shows the results from the tests using both the punch stress and slope between 0.1 and 0.7 displacement fraction. There is no significant maximum stress difference between the sample sets. The dry-cycled sample slope was quite flat and showed a significant difference from both the control and humidity data, but it had a large standard deviation, as did the control slope data.

Seam tape adhesion tests

The seam sealing tape is a very important component of the EMAS system as it ensures environmental protection to the cellular concrete. The adhesion tests were performed to see if temperature cycling and/or extreme cold temperatures would affect the tapes strength or their ability to remain adhered to the block top. Both the initial Tedlar/butyl tape and the newer all-silicone tape were tested.

Each test coupon consisted of two 1-inch-wide by 4-inch-long pieces of top material held together by a 1-inch-wide by 3-inch-long piece of sealing tape.

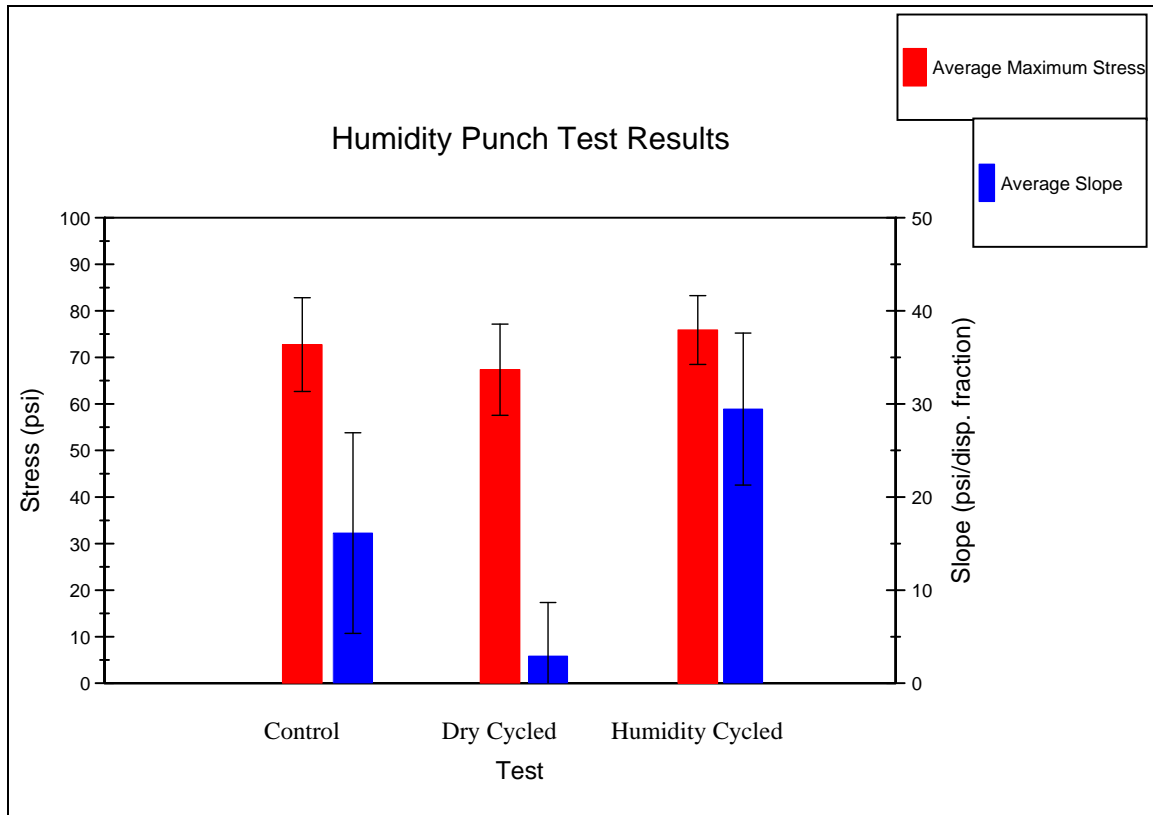


Figure 51. Punch test results for the temperature and humidity testing.

There was a 1/2-inch gap between the plastic top pieces. The tape was adhered to the block top with the same procedure used in the bed and the coupons were inserted into an MTS testing machine with the jaws holding only the top material, as shown in Figure 52. Tension was applied to the coupon at a rate of 0.05 inches per second, resisted only by the tape strength and its bond to the top material. The maximum tensile force was recorded for each test. Five different test conditions were run with five sample repeats at each. The control samples were maintained at room temperature with no cycling. The other samples were all temperature cycled from -50°F to 70°F for 20 cycles and then tested at the temperature shown in Table 5.

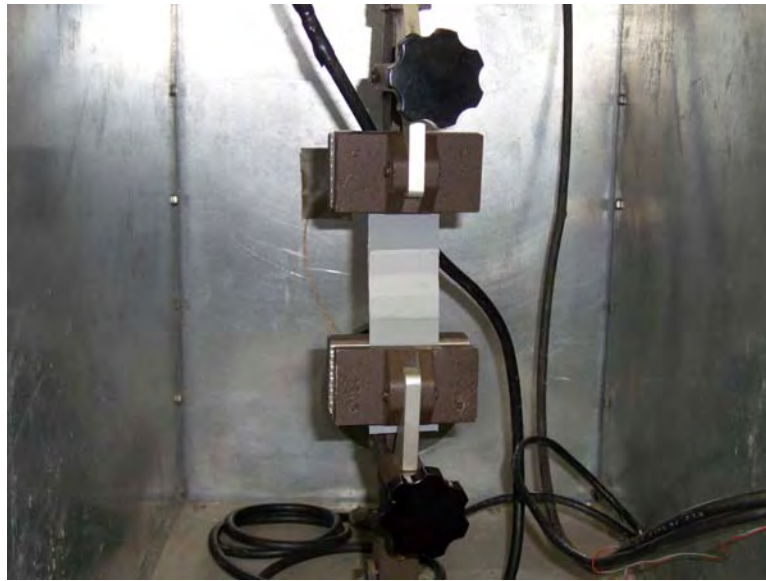


Figure 52. Sealing tape coupon mounted in test fixture.

Table 5. Test conditions for the sealing tape adhesion tests.

Test	Test Temperature (°F)	Cycle Temperature (°F)
Control	Room Temp	No
Room Temp	Room Temp	-50 to 70
0° F	0°	-50 to 70
-20° F	-20	-50 to 70
-50° F	-50	-50 to 70

Seam tape test discussion

Figure 53 shows a typical Tedlar/butyl force/displacement graph for a typical room temperature and a -50°F test. Figure 54 shows the results from all the Tedlar/butyl tape tests.

The first item to note in Figure 54 is that the control and the room temp strengths are identical. This suggests there is not a detrimental effect to tape shear strength from being temperature-cycled. It also can be seen from the figure that the shear strength of the tape increased as the test temperature dropped. This tape is a two-part tape consisting of a Tedlar film on top of a butyl mastic. At room temperature, the failure was usually because the Tedlar slid off the mastic while the mastic would remain attached to the top, as shown in Figure 55. At cold temperatures, the two parts would remain together, creating a stronger entity, and the failure would occur within the Tedlar, as shown in the -20°F test in Figure 56.

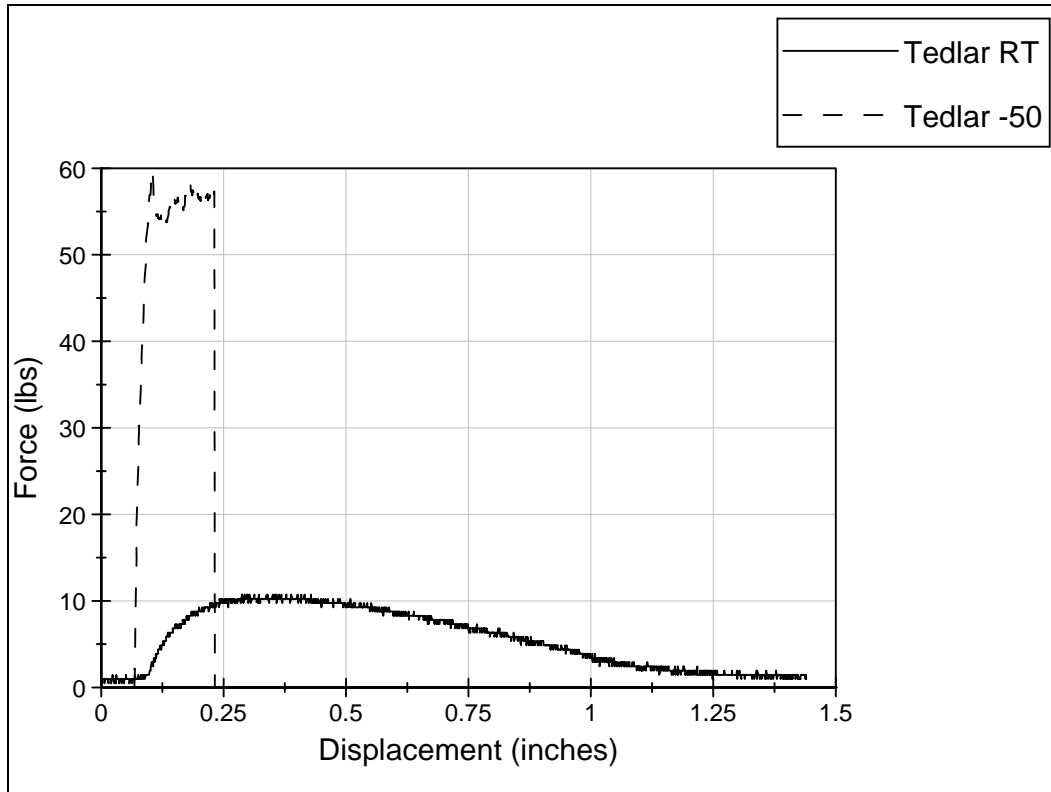


Figure 53. Tedlar/butyl force displacement plot for room temp and - 50° F.

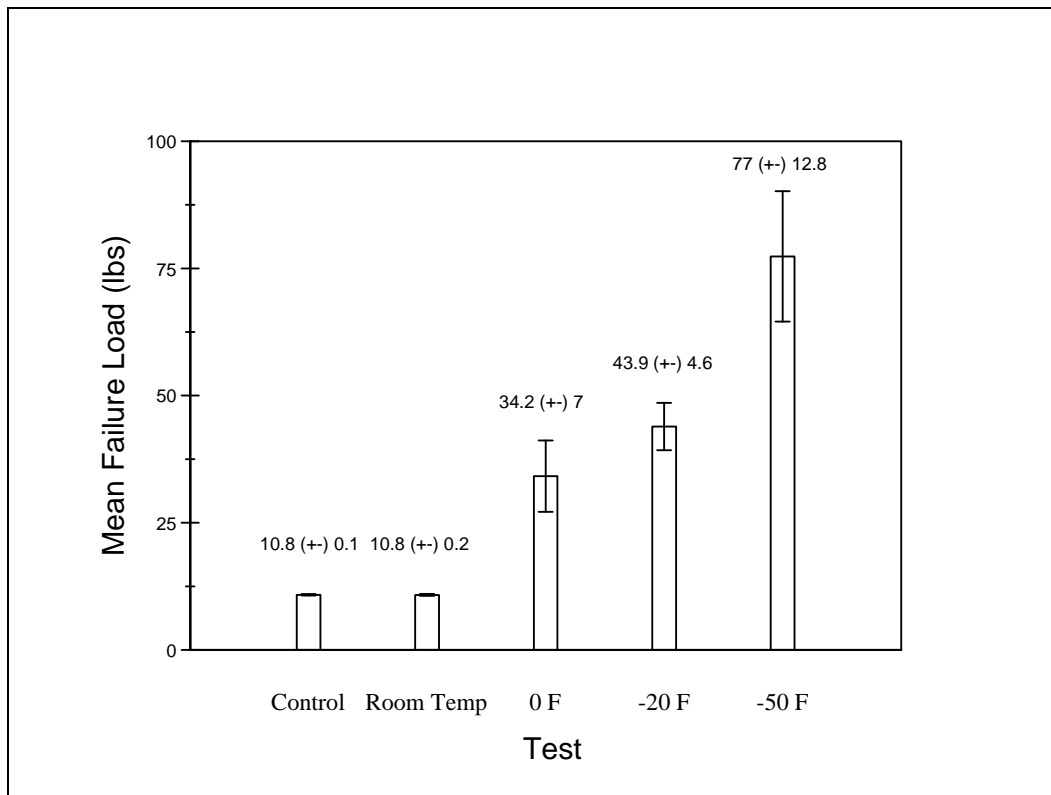


Figure 54. Summary of all Tedlar/butyl tape tests.

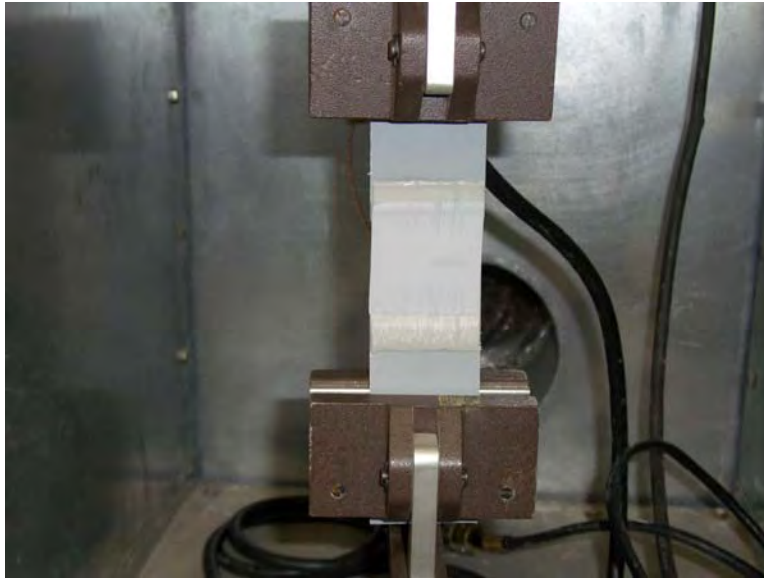


Figure 55. Tedlar/butyl tested at room temperature shows the Tedlar sliding from the butyl mastic.

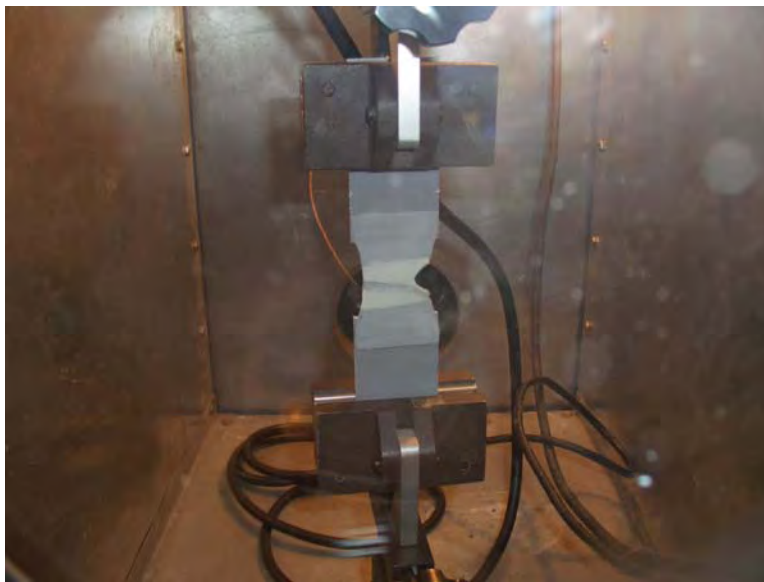


Figure 56. Tedlar/butyl tape tested at a cold temperature showing failure within the Tedlar film and no evidence of sliding off the mastic.

Figure 57 is a typical force/displacement graph for the new silicone seam tape at room temperature and -50°F . Figure 58 shows the results from all the silicone tests. When compared to Figure 54 above, it can be seen that the control and room temperature silicone tape has about twice the failure load of the Tedlar/butyl at room temperature. However, where the Tedlar/butyl increases strength with decreasing temperature, the silicone shows only a very slight increase from room temperature to 0°F , with no further increase until -50°F . The silicone tape also had a much greater

elongation than the Tedlar/butyl did, as shown in Figures 53 and 57, where even the -50° F silicone elongation is greater than the Tedlar room temperature elongation. The silicone tape remained attached to the top material during the tests and failed within the silicone itself, as shown in Figure 59. Overall, the results show there is an increase in the seam tape strength with decreasing temperature in both tapes. This effect is minimal in the newer silicone tape, but that tape is stronger at room temperatures than the older Tedlar/silicone. The silicone has better top adhesion at all temperatures.

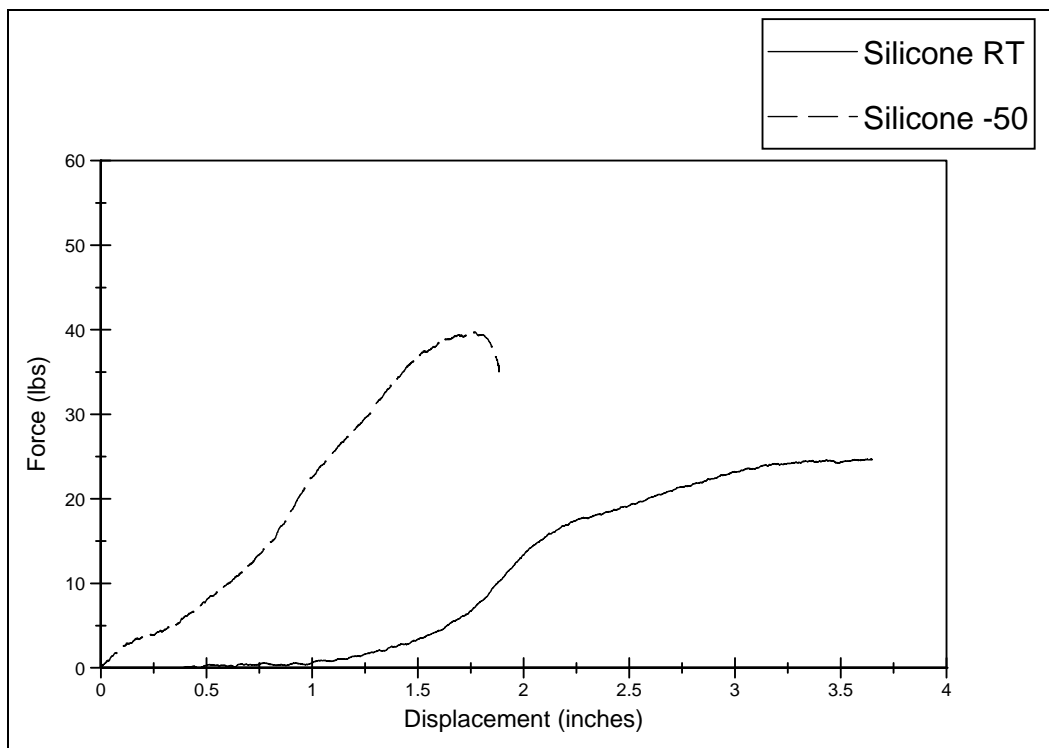


Figure 57. Silicone sealing tape force/displacement graph for room and -50° F temperatures.

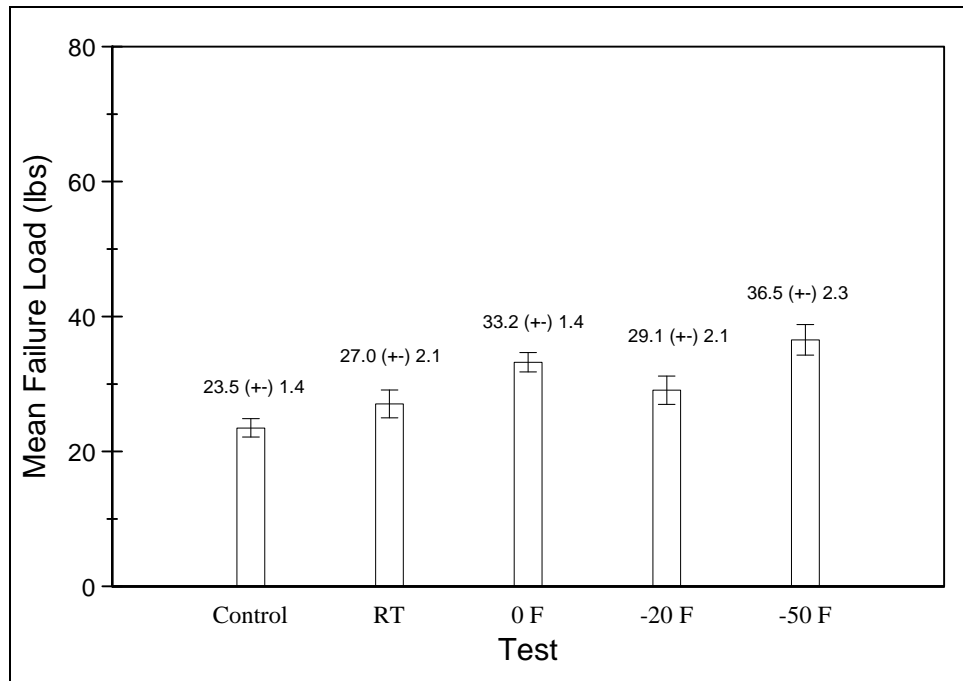


Figure 58. Silicone seam tape summary for all temperatures.



Figure 59. Silicone seam tape at failure. There is no tape slippage from the top material.

Top durability tests

The top on an EMAS block is fabricated to provide a controlled break if it is subjected to an aircraft tire. This top also provides necessary environmental protection to the cellular concrete below, and because materials frequently become more brittle in cold temperatures, a “tool-drop” test sequence was performed to assess the relative effect of an accidental impact to the top in cold temperatures. This series of tests was concerned with environmental protection rather than structural strength.

The test procedure consisted of dropping two types of indenters onto the tops of eight-inch-thick EMAS blocks at room temperature and -15° F and measuring the volume of the dent in the top. The drops were made from different heights starting low enough to just dent the tops and moving up until the indenter broke through the top, and the test stopped. The tops sometimes do not tightly conform to the block beneath because of slight buckling, so the area the top was dropped on was held down to ensure good contact between the top and EMAS block. The indenter was dropped on a new area of the top for each drop, with two repeats at each height.

The indenters are shown in Figures 60 and 61. One was an eye-bolt, dropped ring down, with a somewhat tapered outside diameter to the ring, and one was a purpose-built round ball. The eyebolt had a sharper surface that impacted the top, whereas the ball was much smoother and less pointed. The dimensions and weights of the indenters are listed in Table 6.



Figure 60. Eyebolt drop Indenter.



Figure 61. Spherical drop indenter.

Table 6. Tool drop indenter specifications.

Indenter	Weight (g)	Outer Diameter (mm)	Inner Diameter (mm)	Thickness
Eyebolt	1515	103.1	51.1	26.1
Ball	4011	92.2	—	—

“Tool-drop” test discussion

The damage volume for each indenter was calculated from the depth of the indentation by using an ellipsoidal volume calculation with the eyebolt and a spheroidal volume calculation for the round ball indenter. Because the indenters are different shapes and because we did not measure the rebound velocity, it is best to use the results to compare the temperature effect for each indenter rather than between indenters. Furthermore, since we did not measure the rebound velocity, the K_e shown is the energy just before impact and not the actual energy that went into the damage. The averaged results of the two series are listed in Table 7 along with the kinetic energy associated with the drop height.

Table 7. Average tool drop kinetic energy and damage volume results.

Eyebolt				Round Ball			
Room Temp		-15° F		Room Temp		-15° F	
Ke (Joules)	Damage Volume (mm³)	Ke (Joules)	Damage Volume (mm³)	Ke (Joules)	Damage Volume (mm³)	Ke (Joules)	Damage Volume (mm³)
13.6	1925.5	22.7	1276.3	11.9	0.0	11.9	0
18.1	2890.5	31.7	2382.9	18.0	204.4	18.0	838.3
22.7	4864.5	36.3	4341.4	24.0	1243.0	24.0	1495.3
27.2	7167.6	40.8	7387.0	30.0	2643.7	30.0	2730.7
36.3	9824.5			36.0	4603.3	36.0	3659.5
40.8	10034.3			42.0	6258.9	42.0	4039.7
						48.0	6990.6
						54.0	7688.8

The results are plotted in Figures 62 and 63.

Figure 62 shows there is a strength increase for the eyebolt at -15° F over room temperature throughout the Ke range until breakthrough. Figure 63 shows that the damage from the round ball indenter between the temperatures is the same up to about 30 joules, where the damage becomes slightly less in the cold temperature.

Overall, the data show there is slightly less damage to the top with decreasing temperature.

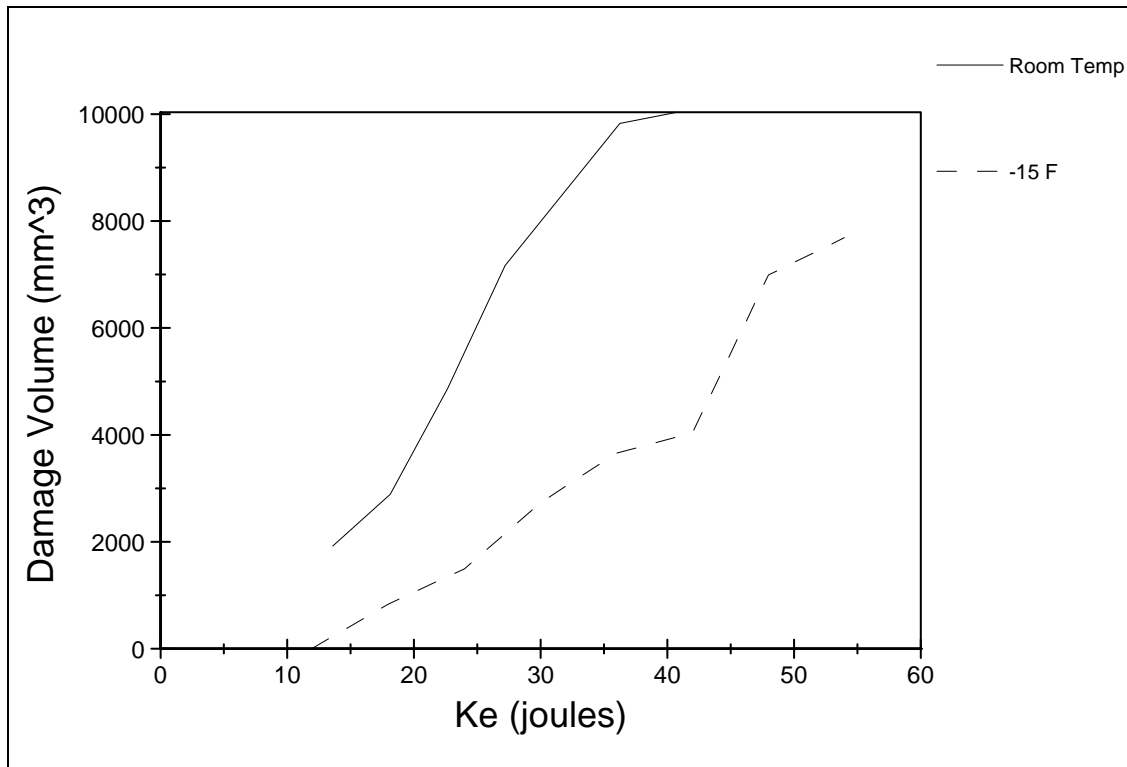


Figure 62. Damage volume versus drop energy for the eyebolt indenter.

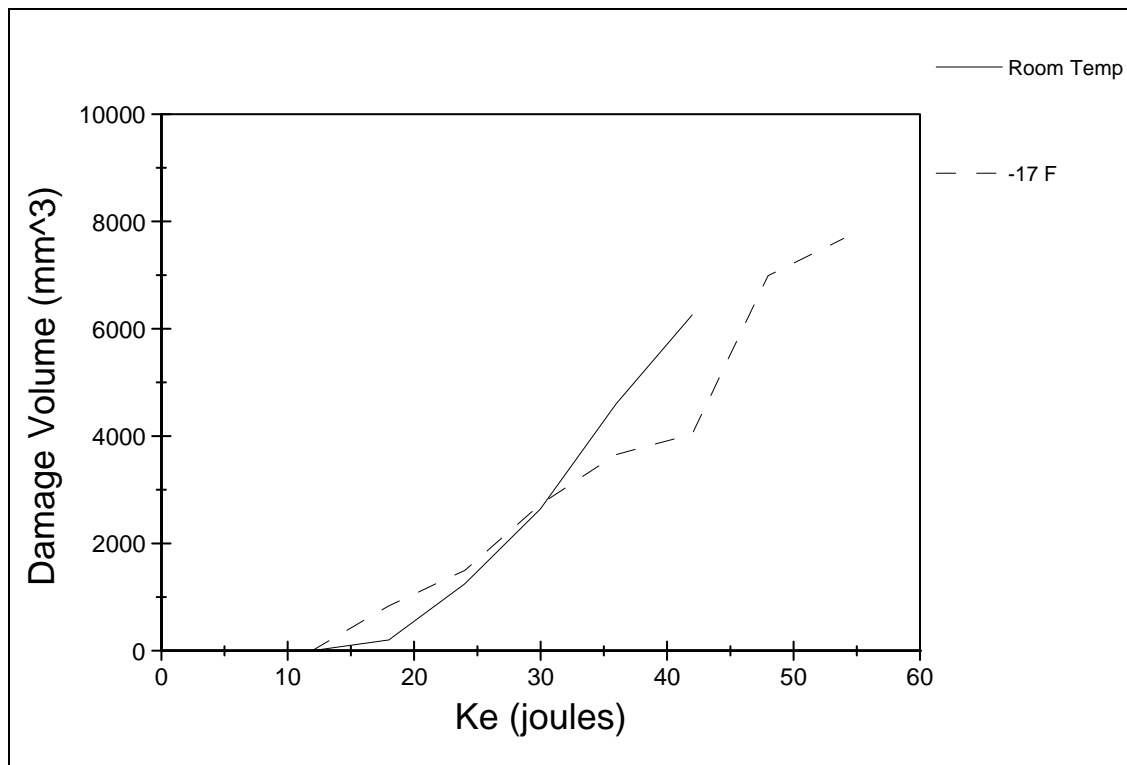


Figure 63. Damage volume versus drop energy for the spherical indenter.